NASA CONTRACTOR
REPORT

NASA CR-179390

NUMERICAL ANALYSIS OF LAMINAR AND TURBULENT INCOMPRESSIBLE FLOWS USING THE FINITE ELEMENT "FLUID DYNAMICS ANALYSIS PACKAGE (FIDAP)"

By Jeong L. Sohn
Universities Space Research Association
4950 Corporate Drive, Suite 100
Huntsville, Alabama 35806

August 1988

Final Contractor Report

Prepared for
NASA, George C. Marshall Space Flight Center
Marshall Space Flight Center, Alabama 35812

TABLE OF CONTENTS

LIST OF ILLUSTRATIONS

LIST OF ILLUSTRATIONS (Concluded)

LIST OF TABLES

CONTRACTOR REPORT

NUMERICAL ANALYSIS OF LAMINAR AND TURBULENT INCOMPRESSIBLE FLOWS USING THE FINITE ELEMENT METHOD

1. INTRODUCTION

Applications of finite element methods to incompressible viscous flows were introduced in the early 1970s [1,2]. In dealing with incompressible flow problems via velocity-pressure formulations, there exist two major obstacles to overcome: (1) the generation of spurious pressure modes by the coupling of velocity and pressure, and (2) oscillatory behaviors (wiggles) of velocity in convection-dominated flows.

Since the mid-1970s, it was recognized that the mixed interpolation (i.e., the interpolation function for pressure as a polynomial of, at least, one order lower than that for velocity) is required to prevent the generation of the spurious pressure modes [3]. Based on the similar motivation, the penalty finite element method was introduced in the late 1970s [4,5]. With this method, the pressure term in the momentum equations could be eliminated by penalizing the incompressibility with a small perturbation and, consequently, the number of equations to be solved could be reduced. As mentioned in Bercovier and Engelman [4] and Hughes et al. [5], the penalty term in momentum equations must be integrated by the reduced integration method to prevent overconstraints of incompressibility. The mathematical investigation of the penalty finite element method with reduced integration has been performed by Oden et al. [6]. As an important improvement of the penalty finite element method, Sani et al. [7] showed that a concept of the mixed interpolation method could be applied to the penalty finite element method. This was done by a consistent application of Galerkin method to the appropriate continuity equation and a consistent integration of all terms in momentum equations. This method is called the penalty finite element integration with a consistent integration. Engelman et al. [8] showed that the reduced integration scheme corresponds to the consistent one only in simple cases, and the consistent integration could provide more accurate solutions than the reduced integration in most situations.

When mixed interpolation polynomials for velocity and pressure are used, a selection of appropriate polynomials is very important [7]. A comparison of various mixed interpolation methods was performed by Huyakorn et al. [9] and they concluded that the bilinear interpolations for velocity and piecewise constant pressure, which is the simplest combination in two-dimensional domain, generates erroneous pressure modes in some cases. Oden and Jacquotte [10] proved both mathematically and numerically that the combination of biquadratic velocity with linear pressure is one of the most stable choices for smooth pressure modes, and the same conclusion was provided by Engelman et al. [8] after numerical experiments in both two- and three-dimensional domain.

It is well-known that the application of conventional Galerkin finite element method to convection-dominated flow problems leads to the centered-difference treatment of the convection term which is a cause of the oscillatory behaviors (wiggles) of velocity or any other flow variables. As mentioned in Gresho and Lee [11], the obvious way to eliminate wiggles is the mesh refinement in the convection-dominated region such that the local Reynolds (or Peclet) number becomes small. On the other hand, the wiggle-free solution could also be obtained by the use of the "upwind"

finite element scheme as an alternative choice of a mesh refinement. The basic idea of upwind finite element method was presented by Christie et al. [12] using modified weighting functions. In this method, the upstream contribution of the weighting function is weighted heavier than that of downstream. This concept was applied to 2-D cases by Heinrich et al. [13,14]. Hughes and Brooks [15] pointed out that the above upwinding scheme could generate excessive numerical diffusion perpendicular to the flow direction in multi-dimensional cases. To overcome this shortcoming, they developed the streamline upwind/Petrov Galerkin method by modifying the weighting function to add numerical diffusion only in the flow direction. The same concept of streamline upwinding has been used by Gresho et al. [16]. Instead of modifying the weight function, they defined an additional term, so-called "balancing tensor diffusivity," which was originated from the second-order difference term in the explicit time integration. They also proved that this term influences only in the flow direction in both steady and unsteady cases.

FIDAP is a finite element code for the analysis of incompressible fluid flows and heat transfer in a multidimensional domain. This code includes both of the available methods for the treatment of velocity-pressure coupling, i.e., penalty and mixed interpolation methods with variable choices of interpolation polynomials for velocity and pressure. Streamline upwind method is included as an option for the convection-dominated flow situations.

2. TEST CASES

The finite element method described in the previous section is applied to the following four examples, i.e.: (1) 2-D laminar flow inside a wall-driven cavity, (2) 2-D laminar flow over a backward-facing step, (3) 2-D turbulent flow over a backward-facing step, and (4) 2-D turbulent flow through a turn-around-duct, are selected. The first three examples are well-known benchmark problems which are useful for the evaluation of any CFD methodologies and there exists computational and/or experimental data for these problems. The fourth case is chosen as an application of the present method to the flow inside a Space Shuttle Main Engine (SSME).

For all test cases, the nine-nodes quadrilateral finite element with linear discontinuous interpolations for pressure (Q_2/P_1) is used. This approach is known to be one of the optimal choices for the treatment of velocity-pressure coupling of the incompressible fluid flow. And, the selected value of the penalty parameter ε is 10^{-6}. Also, the influence of the streamline upwinding (STU) method and its necessary has been investigated.

2-1. 2-D Laminar Flow Inside a Wall-Driven Cavity

As the first test case, a 2-D laminar flow inside a wall-driven cavity is chosen. The essential point of this test case is the prediction of various vortices inside a cavity as shown in Figure 1. The computational solutions of the present study are compared to those worked by Ghia et al. [18] who used the finite difference method of streamline-vorticity formulations with fine (129 x 129 grid points for Re < 3200 and 257 x 257 grid points for Re > 5000) but uniform meshes.

In the present study, 40 x 40 elements (81 x 81 grid points) are used. Fine meshes are used near walls because of viscous boundary layers and the secondary/tertiary recirculating zones of small sizes near corners. The characteristic length of

the smallest element is 0.00326 at four corners and the largest one is 0.03074 at the center of a cavity. The selected Raynolds numbers are 100, 400, 1000, 3200, 5000, 7500, and 10000. To minimize CPU time and optimize initial conditions of the high Reynolds number flow, the restart procedure with the increment of Reynolds number is used. In case of Re = 100, the solution of Stokes flow is chosen as the initial condition. At every selected Reynolds number, the first three iterations for nonlinear solutions are done by the successive substitution method and the quasi-Newton method is chosen after fourth iteration. With these combinations, solutions converged smoothly to 1 percent convergence criteria of the relative velocity, within 4 to 5 iterations at each step. When STU was selected, the number of iterations were unchanged for all Reynolds numbers, but the slope of the convergence curve was steeper than the other.

Figure 2 shows resulting streamline contours for various Reynolds numbers. Influence of STU is also shown at each Reynolds number. Labels of streamline contours are shown in Table 1. Results without STU are generally comparable to those of Ghia et al. with locations and shapes of secondary and tertiary vortices near the bottom corners. As expected, STU generates strong numerical diffusions particularly in high Reynolds number flows. These numerical diffusivities reduce sizes of various vortices. Particularly, the primary vortex in the center of a cavity is seriously influenced by STU.

Pressure contours are shown in Figure 3 with labels in Table 1. STU reduces total pressure differences ($\Delta P = P_{max} - P_{min}$) in all Reynolds numbers. Comparing those results with the results of Gresho et al. [19] for Re = 5000 and 10000, the ΔP's of the present study without STU are bigger than those obtained by Gresho et al., but similar trends of pressure contours are generated in both cases.

Horizontal velocities along the vertical centerline inside a cavity are compared with Ghia et al. in Figure 4. In cases without STU, velocity profiles in all Reynolds numbers excellently agree with Ghia et al. The minimum difference of the peak velocity is 1.00 percent at Re = 100 and the maximum is 1.57 percent at Re = 10000. On the other hand, when STU is selected, the minimum difference is 8.241 percent at Re = 100 and the maximum is 26.10 percent at Re = 10000. Overall velocity profiles with STU are quite different from those without STU at very high Reynolds numbers.

Extreme values of stream functions at various vortices inside a cavity are shown in Table 2. Results of the present study (both with and without STU) are consistently lower than those of Ghia et al. in all Reynolds numbers. For the cases without STU, differences from Ghia et al. are 1.03 percent to 6.40 percent for the primary vortex, 3.28 percent to 18.1 percent for the bottom vortices, and 9.85 percent to 16.67 percent for the top left vortex. Values of extreme stream functions of the primary vortex are higher than those of Gresho et al. This may be simply due to finer grids (h = 0.03074) employed in the central region than Gresho et al. (h = 0.060). Another difference between two cases is the underprediction of bottom vortices of the present study and the overprediction of Gresho et al. Once again, it is shown that STU seriously influences the strengths of vortices.

2-2. 2-D Laminar Flow Over a Backward-Facing Step

Two-dimensional laminar flow over a backward-facing step is selected as the second example. Geometry and boundary conditions are shown in Figure 5. The aspect ratio of the backward-facing step (h) to the overall cross-sectional width is

1:2 and the total length in the horizontal direction is 30 h. A fully-developed parabolic velocity profile is prescribed at the inlet boundary. Predictions of recirculating zones behind a backward-facing step and near the upper wall are compared with experimental measurements of Armaly et al. [20].

30 x 16 elements (61 x 33 grid points) are selected with fine meshes near walls and mixing zone along the centerline. Selected Reynolds numbers are 100, 200, 300, 400, 500, 600, 700, and 800. Here, the Reynolds number is defined by the bulk velocity at the inlet boundary and cross-sectional width of the whole domain which is the same definition as Armaly et al. The same restart procedure as the previous case is adopted. Also, the combination of the successive substitution and quasi-Newton methods is used to stabilize iterations for the nonlinear solutions. Four to five iterations were performed in each step for 1 percent convergence of relative velocity and the same trends of convergence as the previous case were observed.

Figure 6 represents streamline contours for selected Raynolds numbers. Labels of contours are shown in Table 3. The recirculating zone behind a backward-facing step becomes bigger as the Reynolds number increased, and another recirculating zone near the upper wall is generated for Re = 500. STU reduces streamline levels of both recirculating zones. But the reattachment length of the recirculating zone behind a backward-facing zone, x_1, is a little longer than the other case for all Reynolds numbers.

Pressure contours are shown in Figure 7 and Table 3 for selected Reynolds numbers. As Reynolds number increases, the order of magnitude of pressure becomes smaller and the position of maximum pressure moves to downstream. At a fixed Reynolds number, the total pressure difference in the case with STU is bigger than that without STU.

Comparisons with experimental data of Armaly et al. are shown in Figure 8. There is excellent agreement between predicted reattachment lengths and experimental measurements. Discrepancies between computational predictions and experimental data at high Reynolds numbers are originated by the 3-D effects of experiments. The general trend of the curve of x_1 (the reattachment length of the recirculating zone behind a backward-facing step) is the same as that of Kim and Moin [21] who used the finite difference method in the calculations with 101 x 101 grid points. Also, the prediction of beginning (x_2) and ending (x_3) points of the recirculating zone near the upper wall compares satisfactorily with experimental data. By using STU, x_1 becomes longer from 1.3 percent (Re = 800) to 8.0 percent (Re = 100) and x_2 and x_3 are shifted to downstream at low Reynolds number and upstream at high Reynolds number. The width of the recirculating zone near the upper wall is decreased from a maximum of 34.4 percent at Re = 500 and to a minimum of 2.7 percent at Re = 800 by STU.

2-3. 2-D Turbulent Flow Over a Backward-Facing Step

A two-dimensional turbulent flow over a backward-facing step, which is one of the standard test cases of complex turbulent flows presented in the Stanford Conference [22], is chosen. The geometry and boundary conditions are shown in Figure 9. The aspect ratio of the backward-facing step (h) to the whole cross-sectional width is 1:3. Total length in the horizontal direction behind the backward-facing step is 24 h. As previously mentioned, the standard k-ε turbulence model of Launder and

Spalding [17] is used with wall-functions at non-slip walls. Uniform velocity is given at the inlet boundary. Inlet boundary conditions for k and ε are prescribed as follows:

$$k = 0.003\ u_0^2$$

$$\varepsilon = C_\mu\ k^{1.5}\ l^{-1}$$

where $l = 0.03\ h$.

The Reynolds number based on the inlet velocity and the height of a backward-facing step is chosen as 69,610 which represents the same flow condition as Kim et al. [23].

22 x 16 nine-nodes quadrilateral elements (45 x 33 grid points) are used with fine meshes near walls. For the iterative solutions of nonlinear equations, the successive substitution method (acceleration factor = 0.5) is selected. When STU is used, solution was converged to the convergence criteria 0.001 percent of the relative velocity with 65 iterations. Newton-type iterative methods were not suitable to this particular problem because of complex nonlinear terms in the turbulence equations. The streamline upwind (STU) scheme was necessary. When STU was not selected, wiggles are generated in the solution of the ε-equation after 4 to 5 iterations, and velocities are distorted by the influence of these wiggles.

Figure 10 represents streamline contours. The most important parameter to compare with experimental data [22,23] is the reattachment length, x_r, of the separation zone behind a backward-facing step. Predicted x_r in the present study is 5.59. The acceptable value of x_r in the experimental measurement is 7.0 ± 1.0 [23]. Generally, k-ε turbulence model underpredicts x_r by about 20 percent as mentioned in Eaton [24]. In most computational results with k-ε turbulence model, the predicted x_r is in the range of 5.2 to 5.8 [25]. The exact value of x_t depends on the number of grid points and computational methodologies. Also, it depends on various turbulence models [24]. Predicted x_r in the present study is comparable to other computational results with k-ε turbulence model. In addition, although it is not clearly shown in Figure 10, a very small but apparent secondary recirculation exists near the bottom corner of a backward-facing step. This was also predicted by Kaul [26].

In Figure 11, the predicted mean velocity profiles are compared with experimental measurements. Predictions reasonably agree with experimental data downstream, but there exist some differences between predictions and measurements in the separation region and near the wall. Figure 12 shows a comparison of pressure coefficients C_p. In the present study, velocity and pressure at the center of inlet boundary are selected as reference velocity and pressure for the calculation of pressure coefficients. C_p is generally predicted quite well except in the separation zone. The predicted value of C_p in downstream is 0.36.

Contours of turbulent kinetic energy (TKE) are shown in Figure 13. The peak TKE exist at the center of a separation region and steep gradients of TKE exist near the centerline and solid walls. Labels of streamline and TKE contours are shown in Table 4. Predicted TKE's are compared with experimental data in Figure 14. The location of maximum TKE moves closer to the wall in downstream. Differences between predictions and measurements are apparent near the separation and mixing zones. The overprediction of TKE in the separation region may be the cause of the underprediction of the reattachment length. Similar trends of the overprediction of TKE are experienced in other computational results using the k-ε turbulence model [24,25].

2-4. 2-D Turbulent Flow Through a Turn-Around-Duct

This example is selected as an application of the present study to the design of flow paths inside a Space Shuttle Main Engine (SSME). Transition duct between the fuel-side preburner and hot-gas manifolds inside SSME is a 180-degree curved annular turn-around-duct. Experimental studies for turbulent flow through this geometry are done by Sandborn [27] and Sharma and Ostermier [28] using rectangular and axisymmetric shape turn-around-ducts. Experimental apparatus for both cases are shown in Figure 15. Computational results of the present study are compared with these experimental cases.

In case of a rectangular turn-around-duct, the width of a duct (h) is 1.0 and the radius of curvature along the centerline of a duct is 1.0. As shown in Figure 16, two kinds of computational domains are selected. As a first case, the inlet boundary is set at the same location as Sandborn and the uniform velocity (U_{in} = 1.0) has been prescribed as the inlet boundary condition. As the other case, the inlet boundary is set at 5.2 h ahead of the turn and the measured data of mean velocities of Sandborn are prescribed as the inlet boundary condition. The purpose of this study is to investigate the influence of inlet boundary conditions. The wall function is applied along solid boundaries in both cases. And, Reynolds number is selected as 10^5. 40 x 14 finite elements (81 x 29 grid points) and 35 x 14 finite elements (71 x 29 grid points) are used in cases 1 and 2, respectively. The streamline upwind (STU) was necessarily selected to stabilize numerical solutions.

Computational results of cases 1 and 2 are shown in Figures 17 and 18, respectively. Velocity profiles near the inner wall after a turn in case 2 are almost separated from the wall, but no recirculating zone is predicted in both cases which was observed in Sandborn's experiments. This may be originated by the contribution of strong numerical diffusions due to STU in momentum equations. Pressure gradients along the inner wall are steeper than the outer wall in both cases. Gradients of TKEs near the inner wall are steeper than the outer wall in both cases but case 2 has steeper gradients than case 1. Predicted mean velocity profiles of both cases are compared with experimental measurements at various locations in Figure 19, and also, with Chen and Sandborn [29] who used a finite difference method in the same geometry with the second order upwind for momentum equations and a skew upwind for k-ε equations. Difference between predictions and measurements become greater downstream. As expected, predictions of case 2 are better than those of case 1. Pressure coefficients along inner and outer walls are compared with experimental measurements in Figure 20. Both cases are reasonably comparable with experiments.

Computational domain of an axisymmetric shape turn-around-duct is shown in Figure 21. 40 x 14 finite elements (81 x 29 grid points) are used with STU. Uniform velocity (U_{in} = 1.0) is prescribed at the inlet boundary and wall-function is

used along the solid wall. Computational results are shown in Figure 22. Velocity profiles near the inner wall after a turn are physically more unstable than those of a rectangular turn-around-duct. The peak point of the pressure along the inner wall is moved to upstream and gradients of TKEs near the inner wall after a turn are steeper than those of a rectangular turn-around-duct. Predicted pressure coefficients of the present study are compared with experimental measurements of Sharma and Ostermier [28] and computational results of Chen [30] which used higher-order accurate upwinding for momentum equations. Results of the present study are reasonably comparable with experimental data in the upstream of the turn. Differences between predictions of the present study and experimental data in the downstream region may be originated by two main reasons, i.e., (1) numerical diffusions in momentum equations and (2) non-existence of the curvature effects in k-ε turbulence model. As shown in the results of Chen, predictions can be improved by using higher order upwind in momentum equations and modifying k-ε turbulence model to include curvature effects (extended k-ε turbulence model).

3. CONCLUSIONS

Some classical benchmark problens in 2-D laminar and turbulent incompressible fluid flows are tested for the evaluation of numerical accuracy of the finite element, FIDAP, method. As a result of the present study, the following conclusions are drawn:

1. The consistent integration penalty finite element method with Q_2/P_1 elements is efficient to treat velocity-pressure couplings of the incompressible fluid flow.

2. Streamline upwinding (STU) produces too strong numerical diffusions in the high Reynolds number laminar flow, particularly, inside a wall-driven cavity.

3. When STU is not selected, numerical results of the present study on laminar flow are in good agreement with other CFD solutions and experimental data.

4. STU is essential to the computation of turbulent flow because it stabilizes numerical solutions of k-ε equations. However, as shown in the case of the flow through a turn-around-duct, momentum equations are still strongly influenced by STU. Therefore, numerical diffusions in the velocity field must be minimized by applying higher-order upwinding techniques to momentum equations.

5. Results of the present study on turbulent flow correspond to the general trends of other computational solutions of the standard k-ε turbulence model. Differences from experimental data in both test cases for turbulent flow are mainly caused by the limitations of the standard k-ε turbulence model on the recirculating and curved flow. Therefore, the advanced turbulence models are necessarily required for the accurate predictions of complex turbulent flows. The incorporation of such advanced turbulence models in the finite element code, FIDAP, is one of several tasks requiring a continuous study.

REFERENCES

1. Oden, J. T., and Wellford, L. C.: Analysis of Flow of Viscous Fluids by the Finite Element Method. AIAA J., Vol. 10, 1972, pp. 1590-1599.

2. Taylor, C., and Hood, P.: A Numerical Solution of the Navier-Stokes Equations Using the Finite Element Technique. Computers and Fluids, Vol. 1, 1973, pp. 73-100.

3. Hood, P., and Taylor, C.: Navier-Stokes Equations Using Mixed Interpolation. Finite Elements Methods in Flow Problems, Edited by J. T. Oden. O. C. Zienkiewicz, K. H. Gallagher, and C. Taylor, UAH Press, 1974, pp. 121-132.

4. Bercovier, M., and Engelman, M.: A Finite Element for the Numerical Solution of Viscous Incompressible Flows. J. Comp. Phys., Vol. 30, 1979, pp. 181-201.

5. Hughes, T. J. R., Liu, W. K., and Brooks, A.: Review of Finite Element Analysis of Incompressible Viscous Flows by Penalty Function Formulation. J. Comp. Phys., Vol. 30, 1979, p. 1-60.

6. Oden, J. T., Kikuchi, N., and Song, Y. J.: Penalty-Finite Element Methods for the Analysis of Stokesian Flows. Comp. Meth. Appl. Mech. Eng., Vol. 31, 1982, pp. 297-329.

7. Sani, R. L., Gresho, P. M., Lee, R. L., and Griffiths, D. F.: The Cause and Cure (?) of the Spurious Pressure Generated by Certain FEM Solutions of the Incompressible Navier-Stokes Equations: Part 1. Int. J. Num. Meth. Fluids, Vol. 1, 1981, pp. 17-43.

8. Engelman, M., Sani, R. L., Gresho, P. M., and Bercovier, M.: Consistent Versus Reduced Integration Penalty Methods for Incompressible Media Using Several Old and New Element. Int. J. Num. Meth. Fluids, Vol. 2, 1982, pp. 25-42.

9. Huyakorn, P. S., Taylor, C., Lee, R. L., and Gresho, P. M.: A Comparison of Various Mixed-Interpolation Finite Elements in the Velocity-Pressure Formulation of the Navier-Stokes Equations. Computers and Fluids, Vol. 6, 1978, pp. 25-35.

10. Oden, J. T., and Jacquotte, O. P.: Stability of Some Mixed Finite Element Methods for Stokesian Flows. Comp. Meth. Appl. Mech. Eng., Vol. 43, 1984, pp. 231-247.

11. Gresho, P., and Lee, R. L.: Don't Suppress the Wiggles - They're Telling You Something. Computers and Fluids, Vol. 9, 1981, pp. 223-253.

12. Christie, I., Griffiths, D. F., Mitchell, A. R., and Zienkiewicz, O. C.: Finite Element Methods for Second Order Differential Equations with Significant First Derivatives. Int. J. Num. Meth. Eng., Vol. 10, 1976, pp. 1389-1396.

13. Heinrich, J. C., Huyakorn, P. S., Zienkiewicz, O. C., and Mitchell, A. R.: An "Upwind" Finite Element Scheme for Two-Dimensional Convective Transport Equation. Int. J. Num. Meth. Eng., Vol. 11, 1977, pp. 131-143.

14. Heinrich, J. C., and Zienkiewicz, O. C.: Quadratic Finite Element Schemes for Two-Dimensional Convective-Transport Problems. Int. J. Num. Meth. Eng., Vol. 11, 1977, pp. 1831-1844.

15. Brooks, A. N., and Hughes, T. J. R.: Streamline Upwind/Petrov-Galerkin Formulations for Convection Dominated Flows with Particular Emphasis on the Incompressible Navier-Stokes Equations. Comp. Meth. Appl. Mech. Eng., Vol. 32, 1982, pp. 199-259.

16. Gresho, P. M., Chan, S. T., Lee, R. L., and Upson, G. D.: A Modified Finite Element Method for Solving the Time-Dependent, Incompressible Navier-Stokes Equations, Part 1: Theory. Int. J. Num. Meth. Fluids, Vol., 4, 1984, pp. 557-598.

17. Launder, B. E., and Spalding, D. B.: The Numerical Computation of Turbulent Flows. Comp. Meth. Appl. Mech. Eng., Vol. 3, 1974, pp. 269-289.

18. Ghia, U., Ghia, K. N., and Shin, C. T.: High-Re Solutions for Incompressible Flow Using the Navier-Stokes Equations and a Multi-Grid. J. Comp. Phys., Vol. 48, 1982, pp. 387-411.

19. Gresho, P. M., Chan, S. T., Lee, R. L., and Upson, C. D.: A Modified Finite Element Method for Solving the Time-Dependent Imcompressible Navier-Stokes Equations, Part 2: Applications. Int. J. Num. Meth. Fluids, Vol. 4, 1984, pp. 619-640.

20. Armaly, B. F., Durst, F., Pereira, J. C. F., and Schonung, B.: Experimental and Theoretical Investigation of Backward-Facing Step Flow. J. Fluid Mech., Vol. 127, 1983, pp. 473-496.

21. Kim, J., and Moin, P.: Application of a Fractional-Step Method to Incompressible Navier-Stokes Equations. J. Comp. Phys., Vol. 59, 1985, pp. 308-323.

22. Eaton, J. K., and Johnston, J. P.: Backward-Facing Step Flow. Proc. 1980-81 AFOSR-HTTM-Stanford Conference on Complex Turbulent Flows: Comparison of Computation and Experiment, Vol. I, 1981, pp. 275-278.

23. Kim, J., Kline, S. J., and Johnston, J. P.: Investigation of a Reattaching Turbulent Shear Layer: Flow Over a Backward-Facing Step. J. Fluid Eng., ASME Tran., Vol. 102, 1980, pp. 302-308.

24. Eaton, J. K.: Incompressible Separated Flows - Internal Flows: Backward-Facing Step. Proc. 1980-91 AFOSR-HTTM-Stanford Conference on Complex Turbulent Flows: Comparison of Computation and Experiment, Vol. II, 1982, pp. 886-904.

25. Launder, B. E.: Influence of Numerics and Computors Variance in the Computation of Complex Turbulent Flows. Proc. 1980-91 AFOSR-HTTM-Stanford Conference on Complex Turbulent Flows: Comparison of Computation and Experiment, Vol. II, 1982, pp. 843-862.

26. Kaul, U.: An Implicit Finite-Difference Code for a Two-Equation Turbulente Model for Three-Dimensional Flows. NASA TR-86752, 1985.

27. Sandborn, V. A.: Measurements in a 180 Degree, Small Radius of Curvature Water Channel. Proc. of the 5th SSME CFD Workshop, NASA/MSFC, Huntsville, Alabama, April 21-23, 1987.

28. Sharma, L. K., and Ostermier, B. J.: Flowfield Characteristics of an Axi-symmetric 180-degree Turnaround Duct. Proc. of the 5th SSME CFD Workshop, NASA/MSFC, Huntsville, Alabama, April 21-23, 1987.

29. Chen, Y. S., and Sandborn, V. A.: Computational and Experimental Study of Turbulent Flows in 180 Degree Bends. AIAA Paper 86-1516, 1986.

30. Chen, Y. S.: Development of a High Accuracy Finite Difference Upwind Differencing Scheme for Viscous Flow Computations. Proc. of the 5th SSME CFD Workshop, NASA/MSFC, Huntsville, Alabama, April 21-23, 1987.

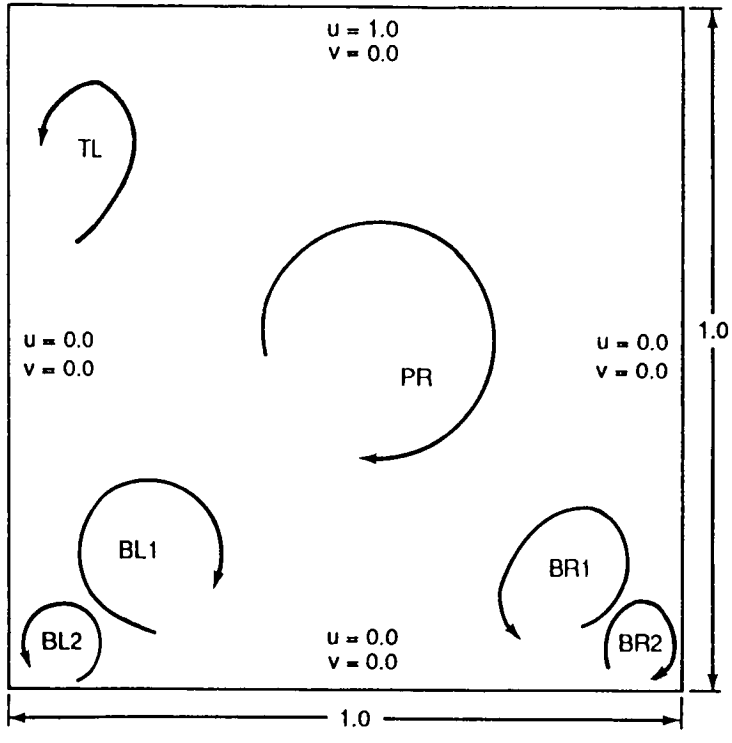

Figure 1. Geometry and boundary conditions of 2-D laminar flow inside a wall-driven cavity.

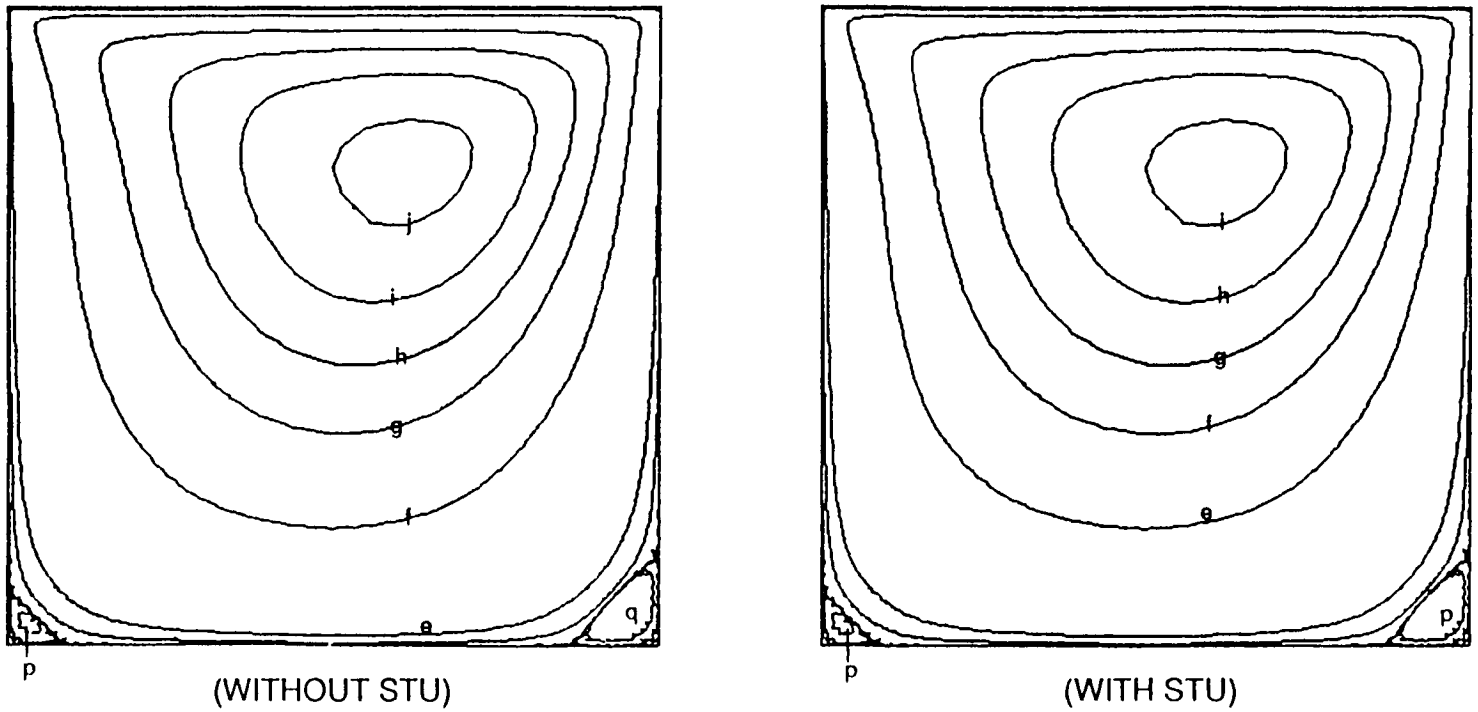

(a) Re = 100

Figure 2. Streamline contours of 2-D laminar flow inside a wall-driven cavity.

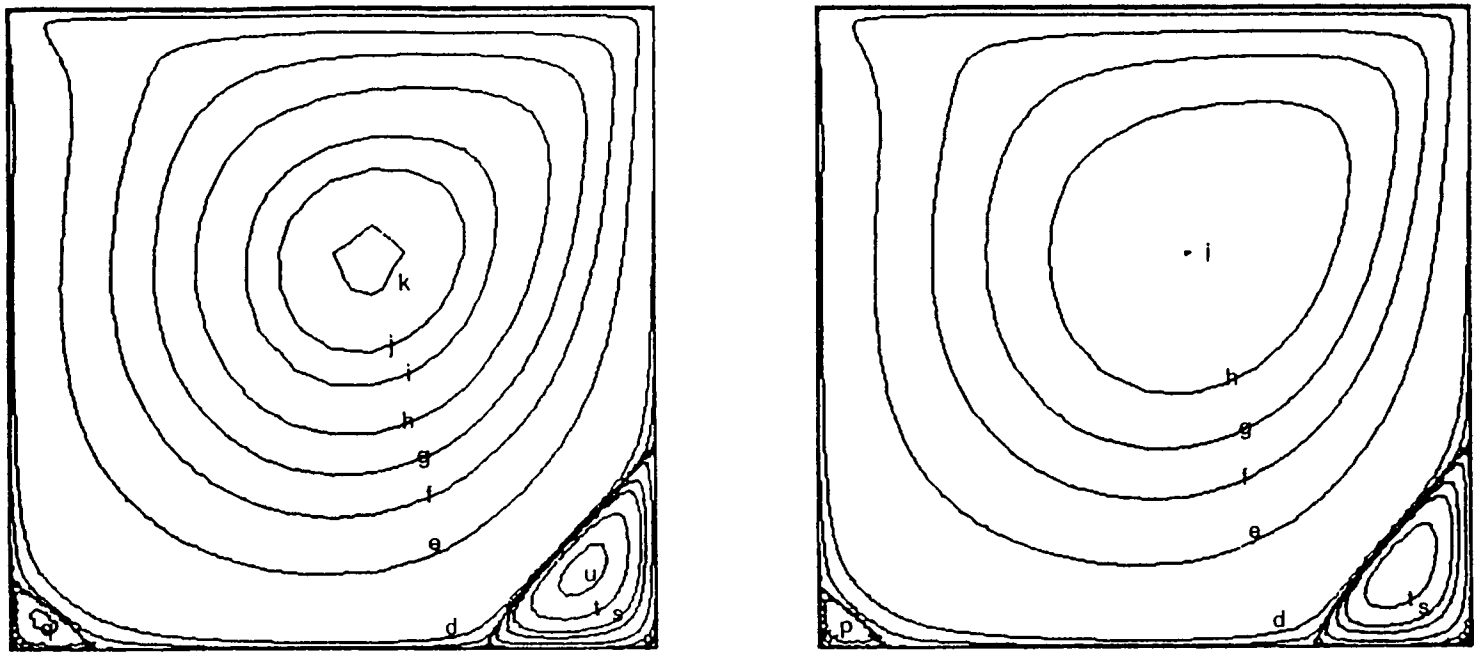

(WITHOUT STU) (WITH STU)

(b) Re = 400

Figure 2. (Continued)

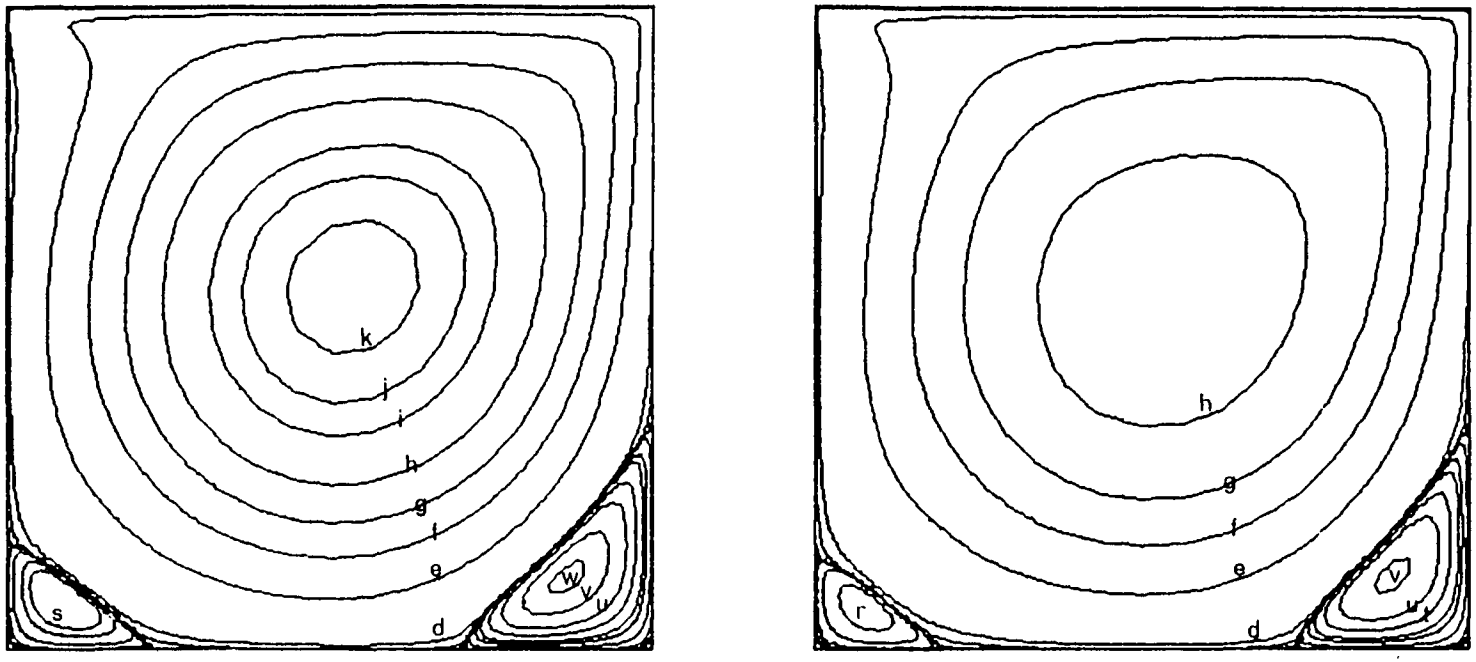

(WITHOUT STU) (WITH STU)

(c) Re = 1000

Figure 2. (Continued)

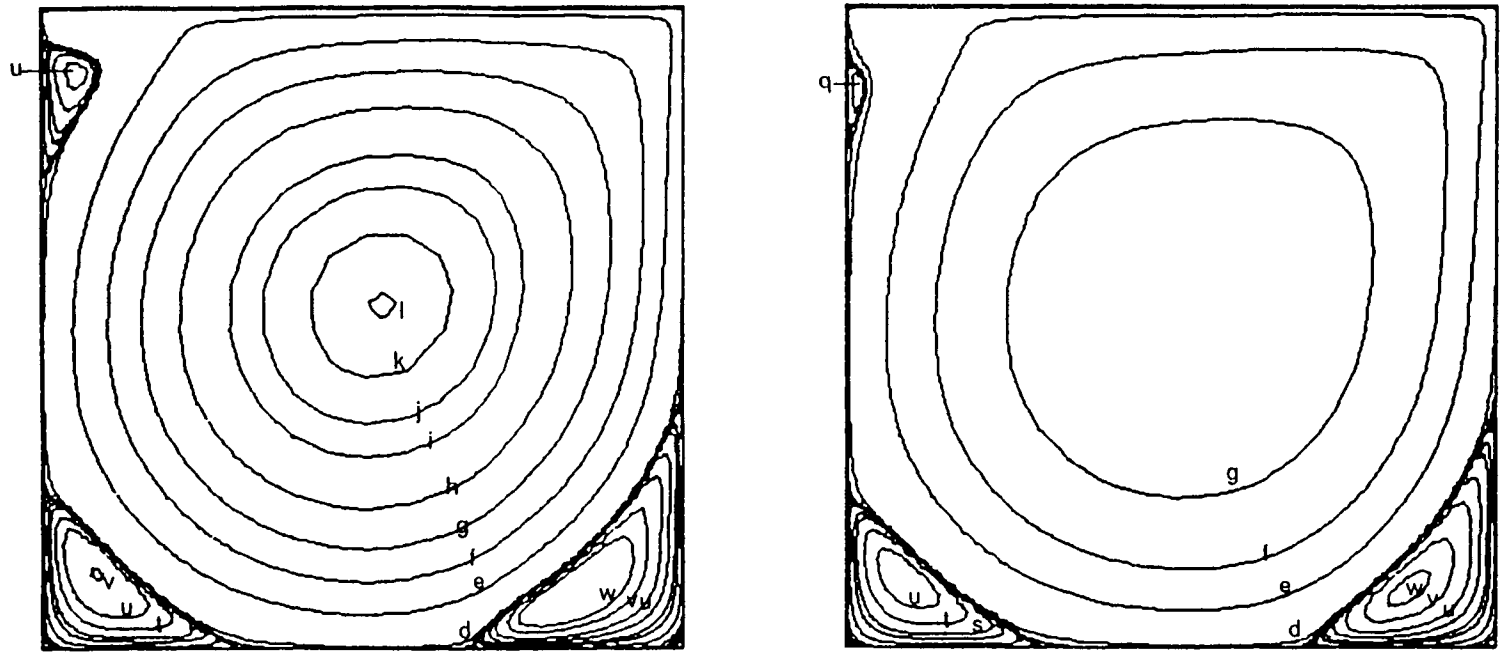

(WITHOUT STU) (WITH STU)

(d) Re = 3200

Figure 2. (Continued)

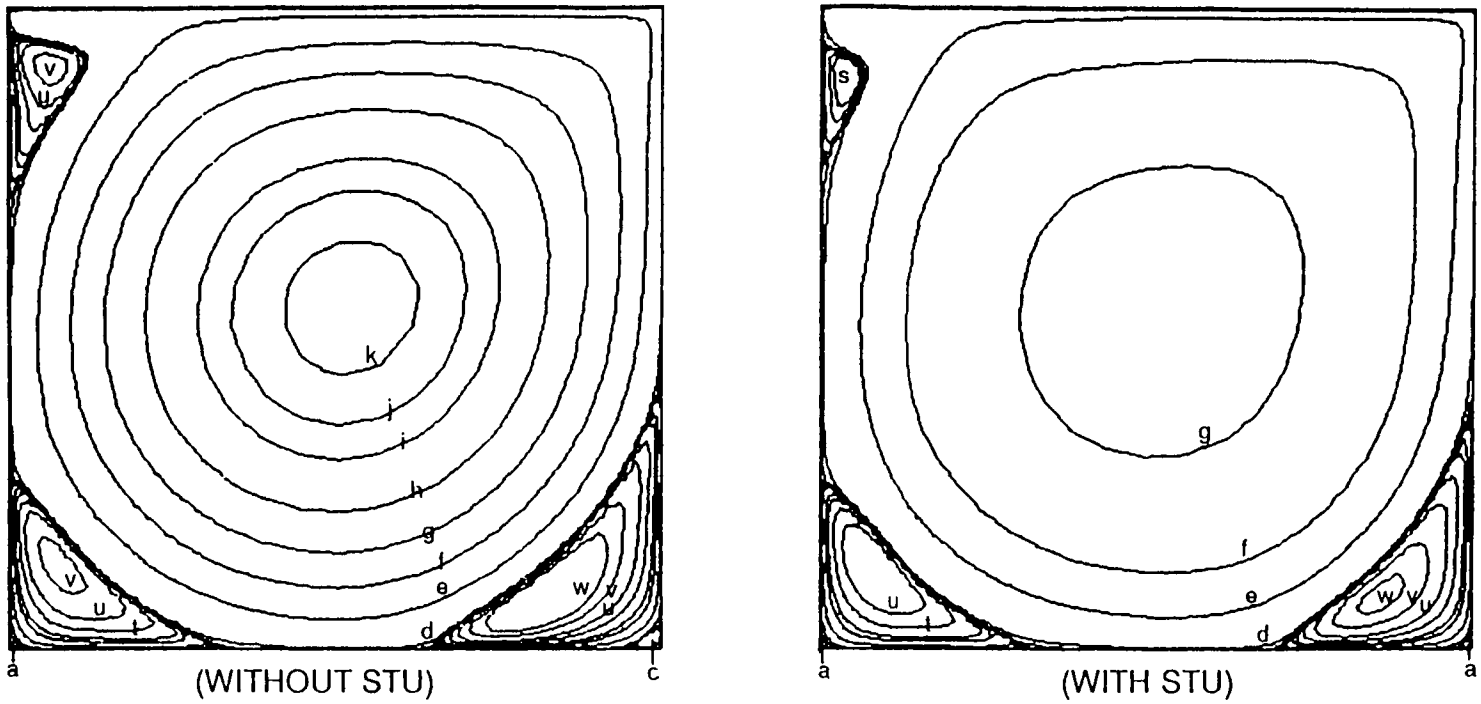

(e) Re = 5000

Figure 2. (Continued)

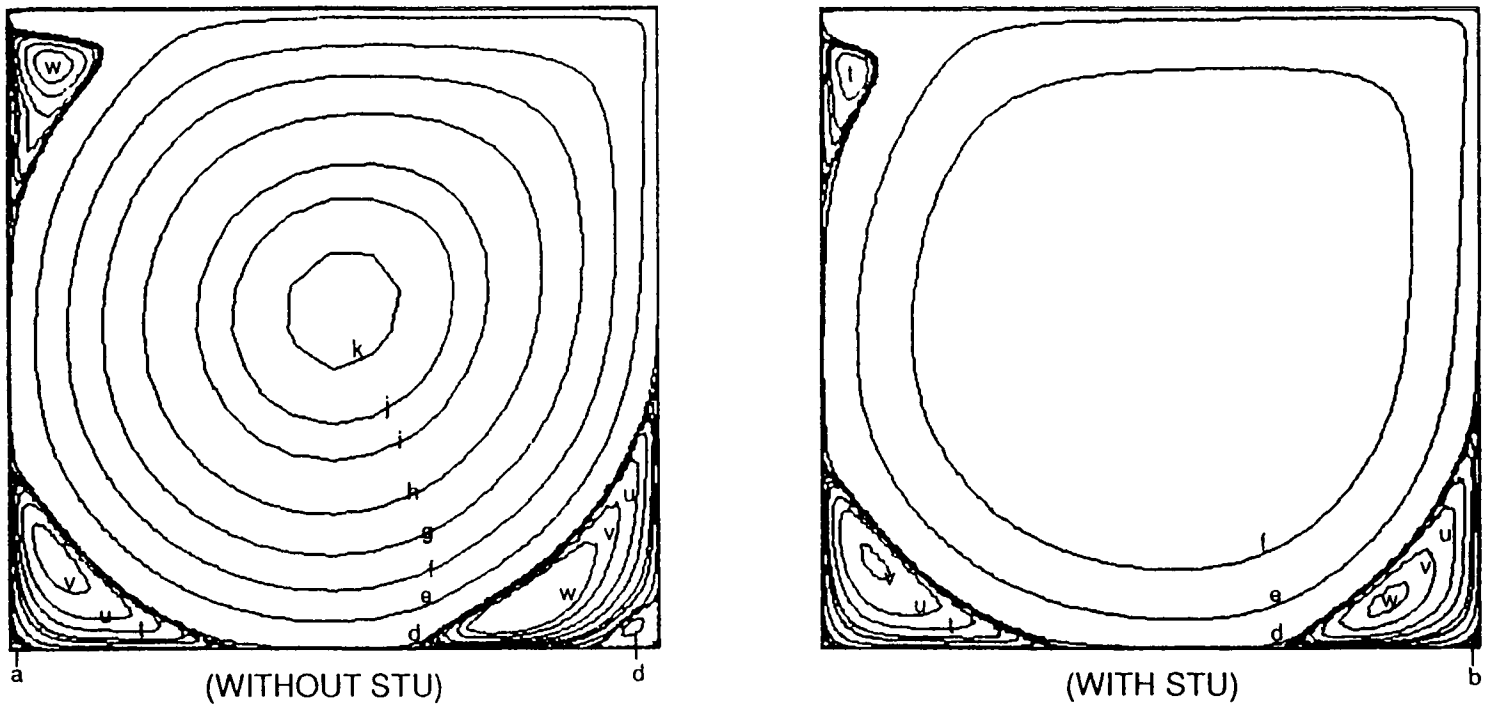

(f) Re = 7500

Figure 2. (Continued)

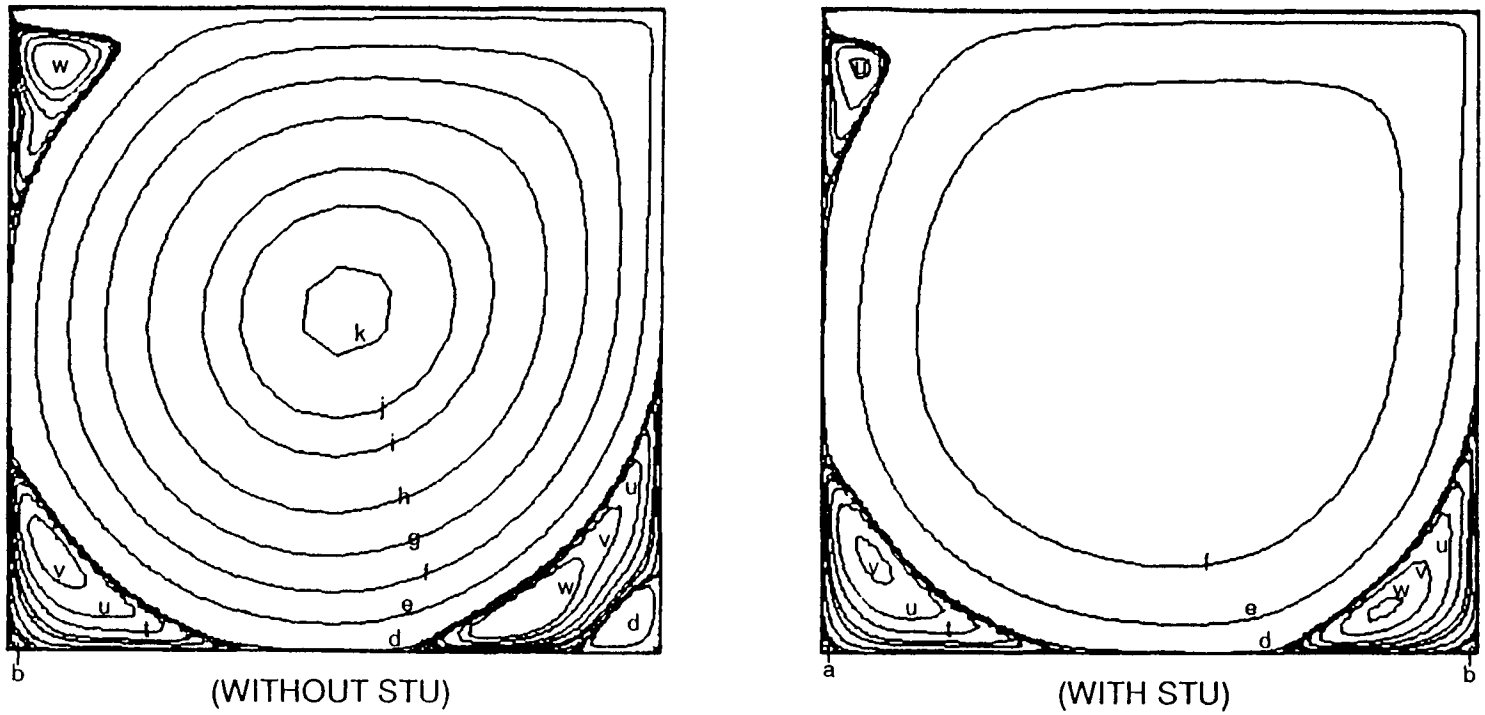

(g) Re = 10,000

Figure 2. (Concluded)

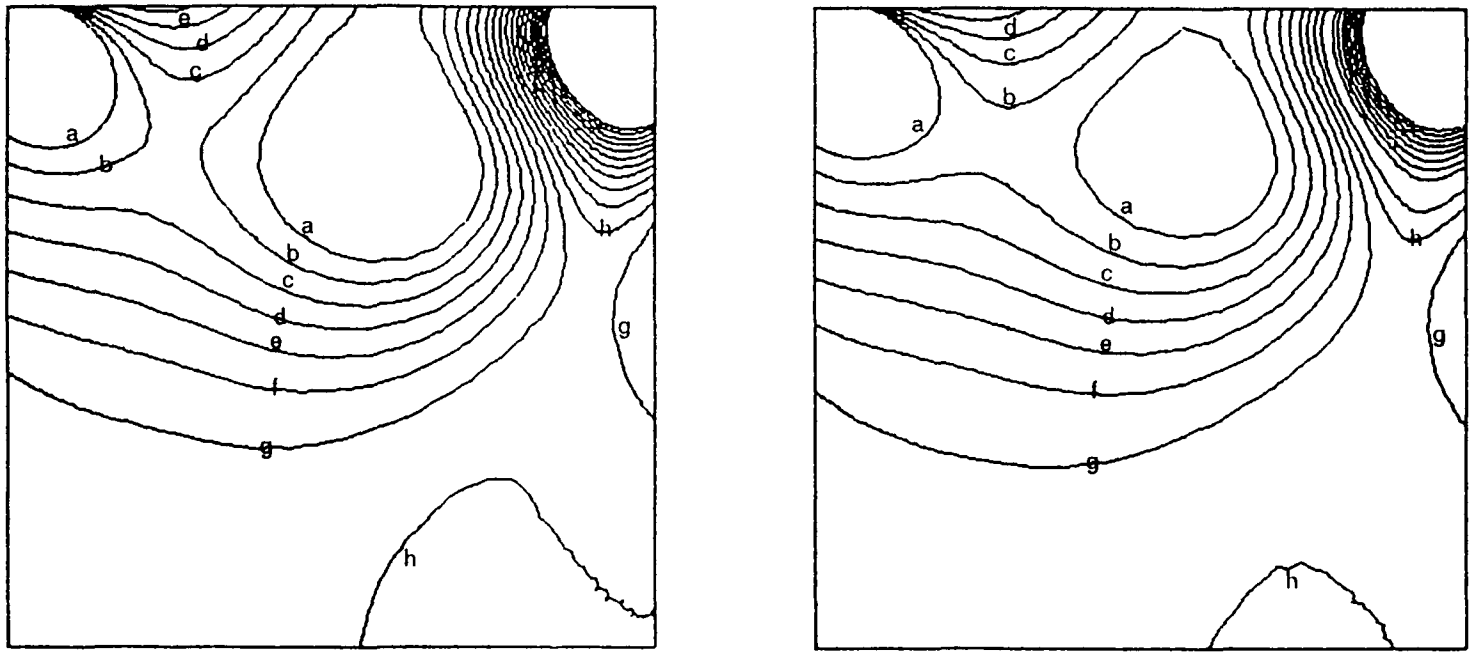

(a) Re = 100

Figure 3. Pressure contours of 2-D laminar flow.

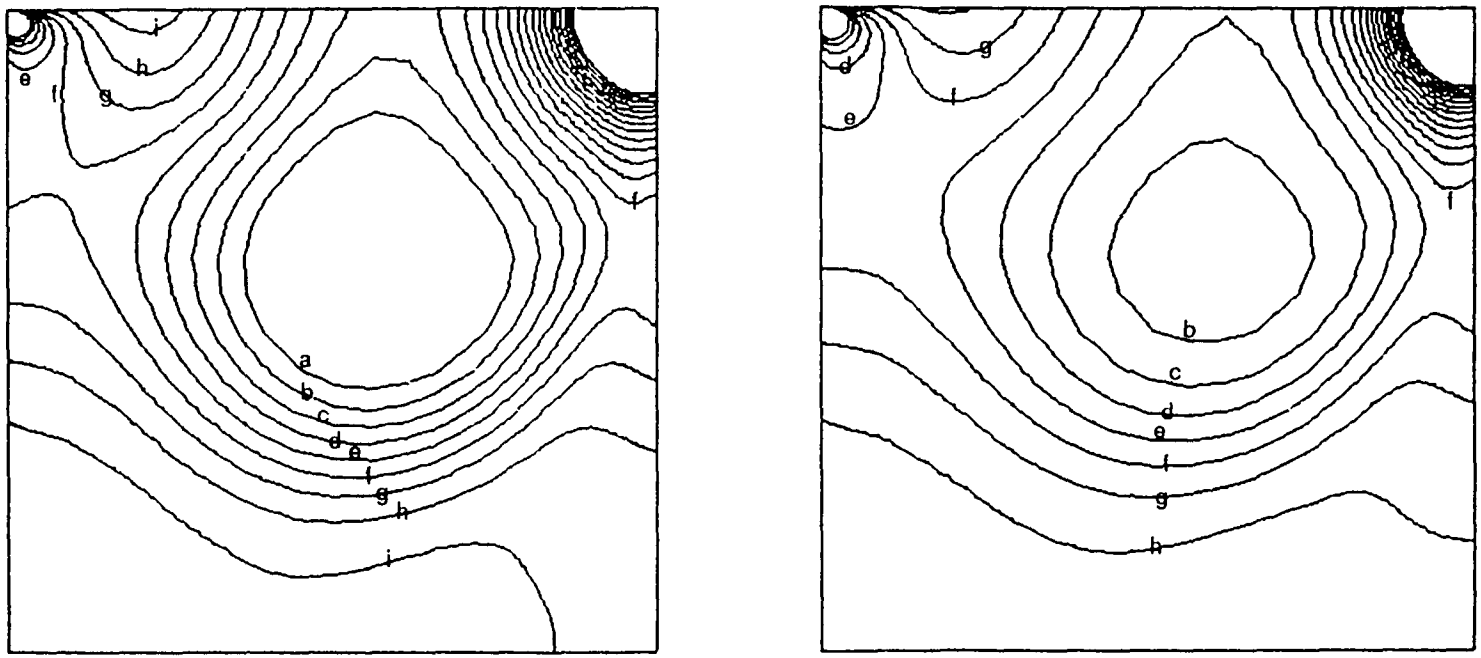

(b) Re = 400

Figure 3. (Continued)

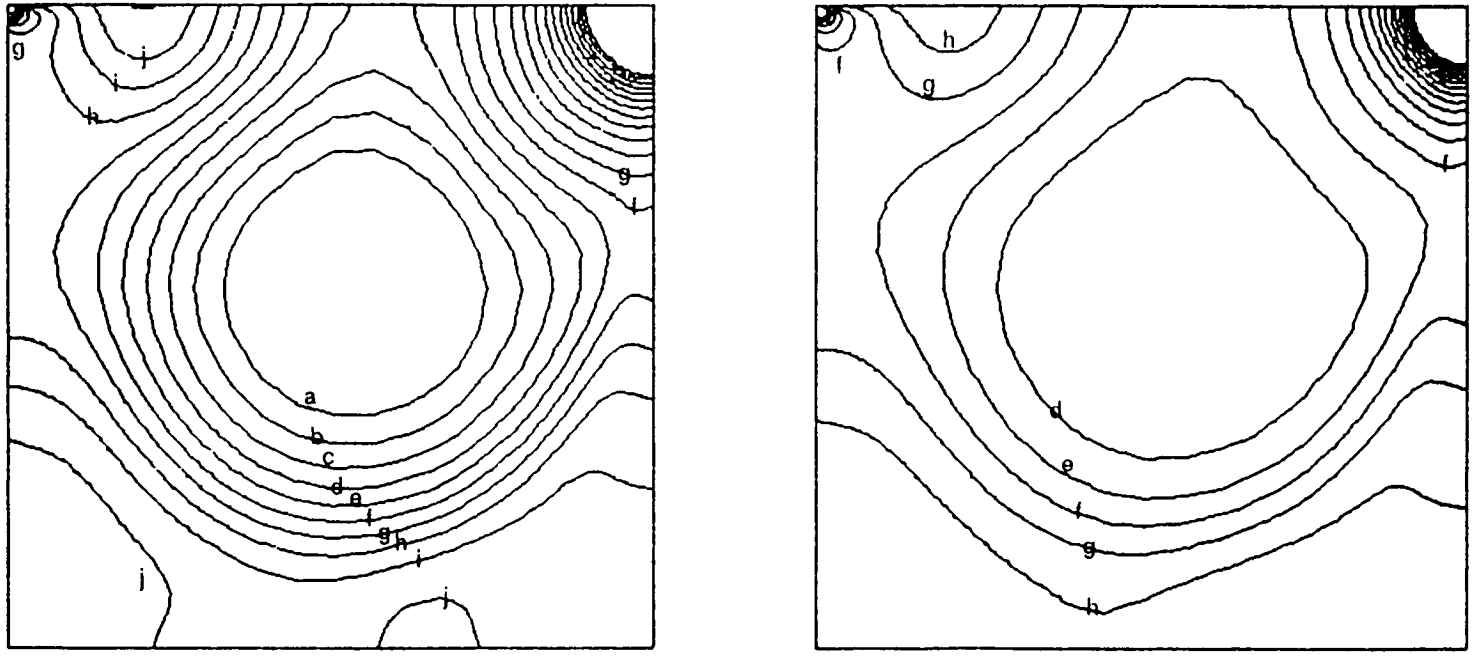

(c) Re = 1000

Figure 3. (Continued)

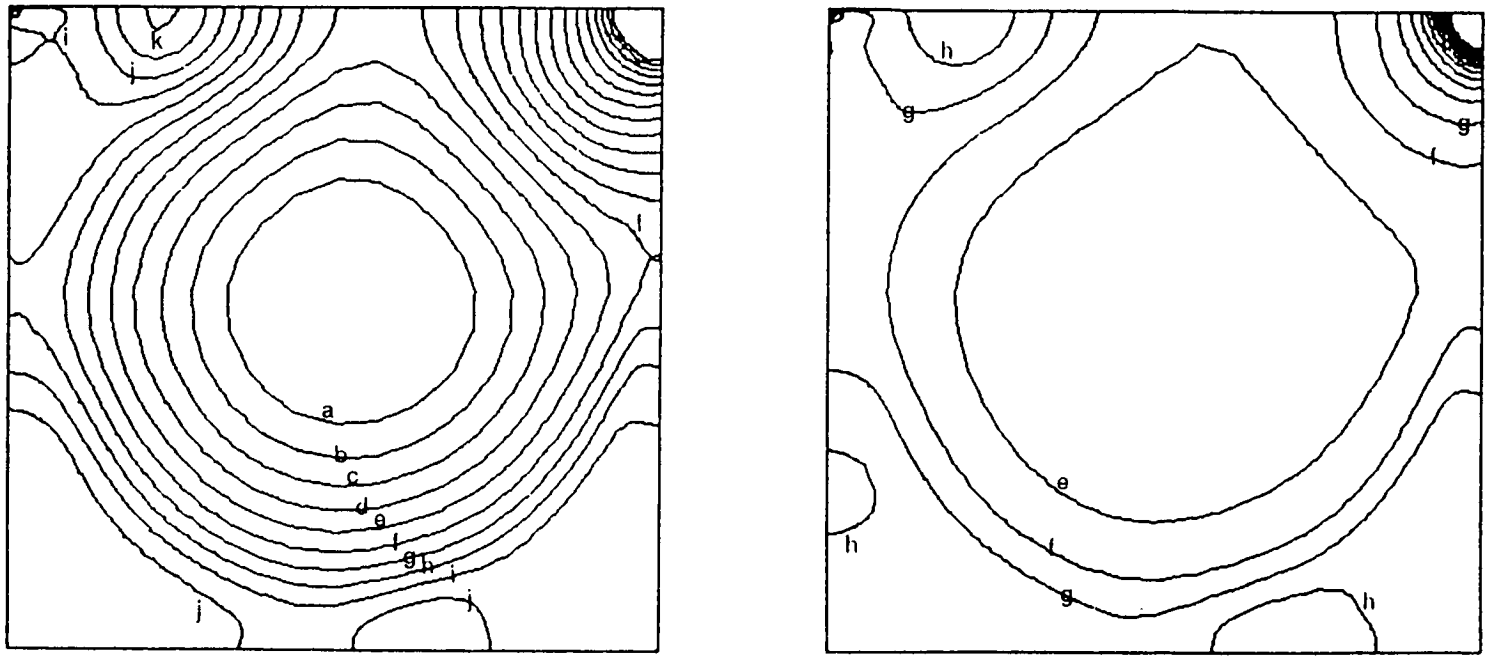

(WITHOUT STU) (WITH STU)

(d) Re = 3200

Figure 3. (Continued)

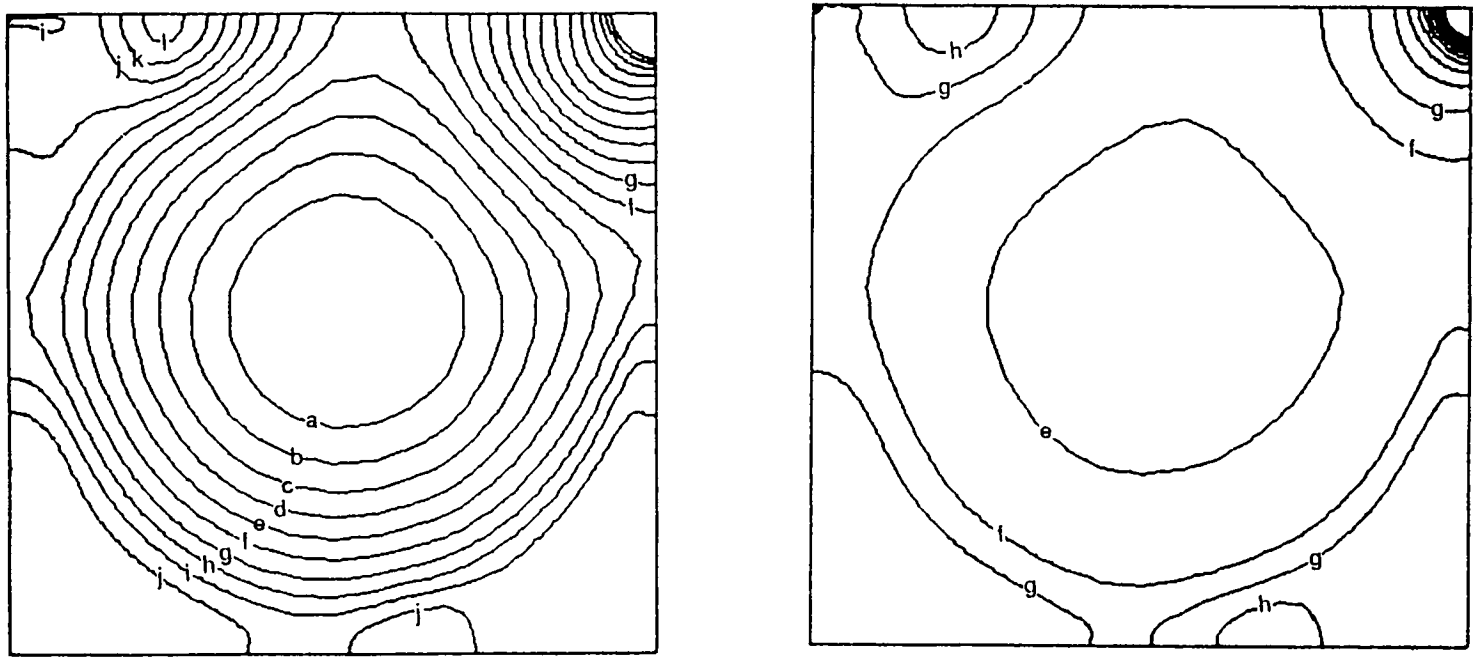

(WITHOUT STU) (WITH STU)

(e) Re = 5000

Figure 3. (Continued)

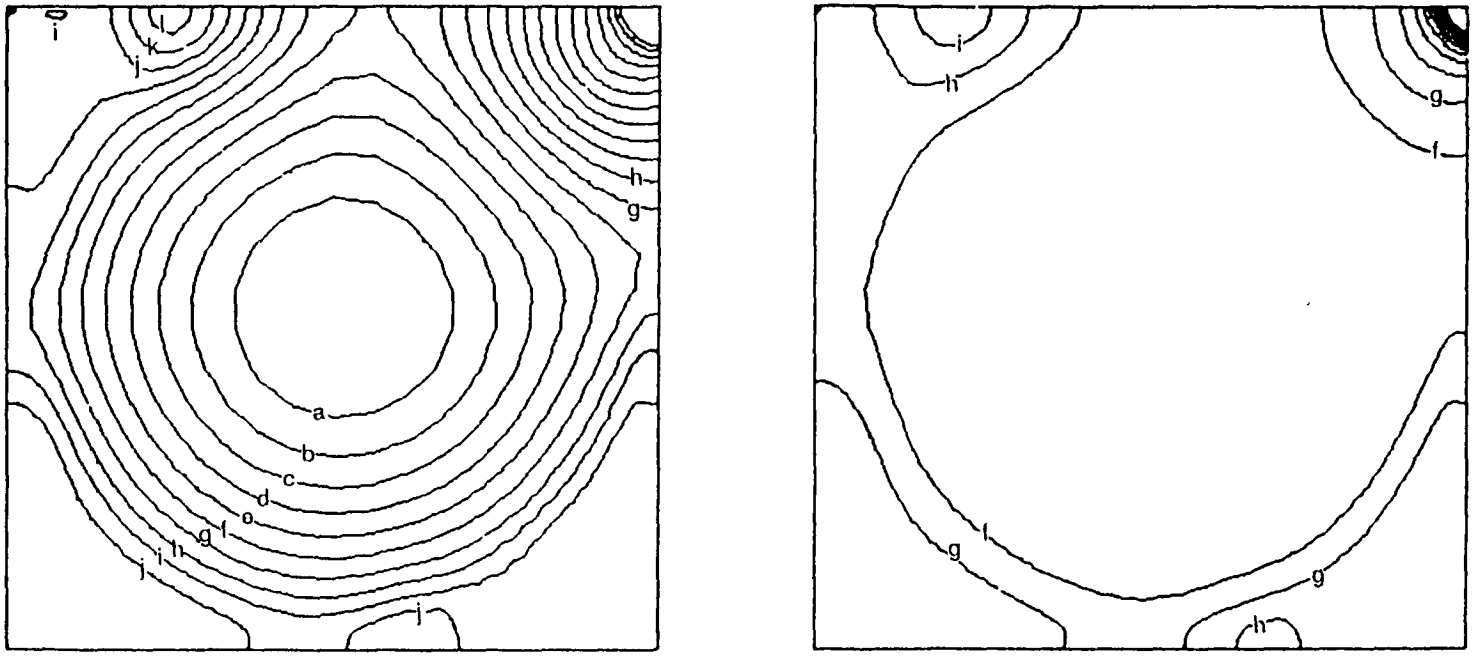

(WITHOUT STU) (WITH STU)

(f) Re = 7500

Figure 3. (Continued)

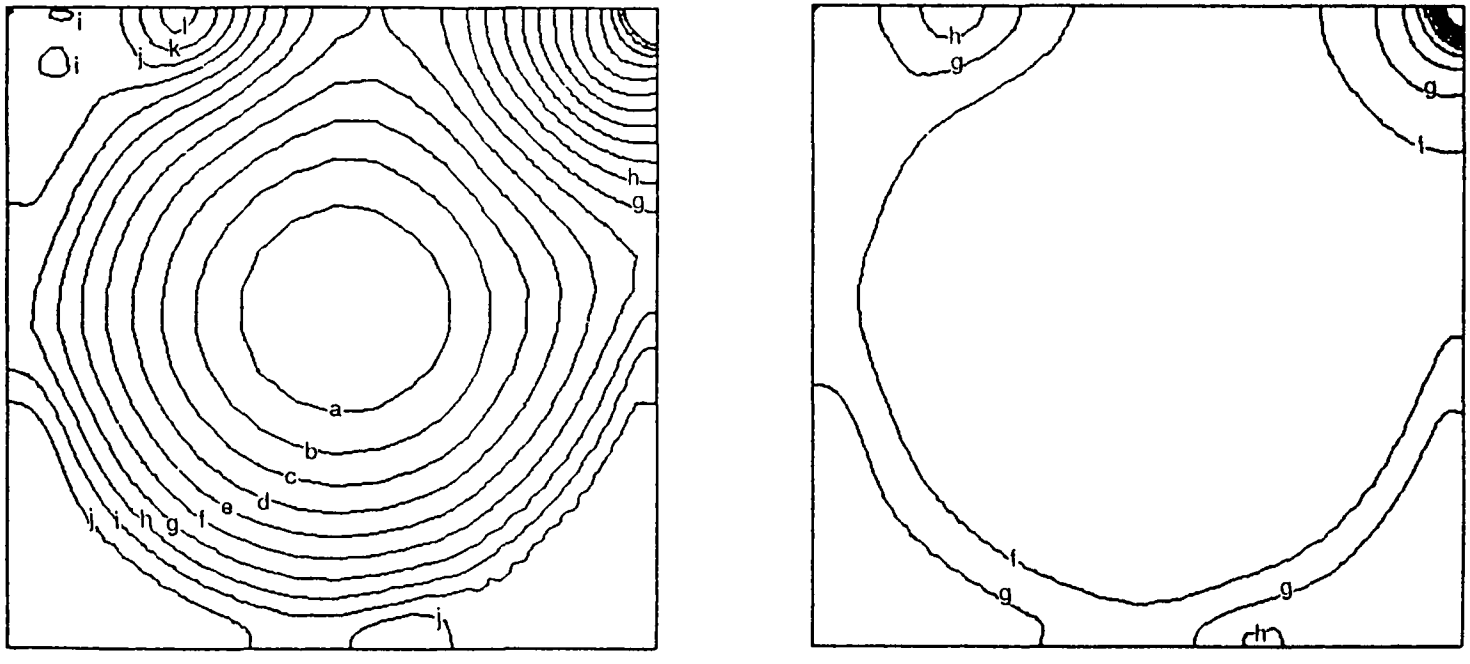

(g) Re = 10,000

Figure 3. (Concluded)

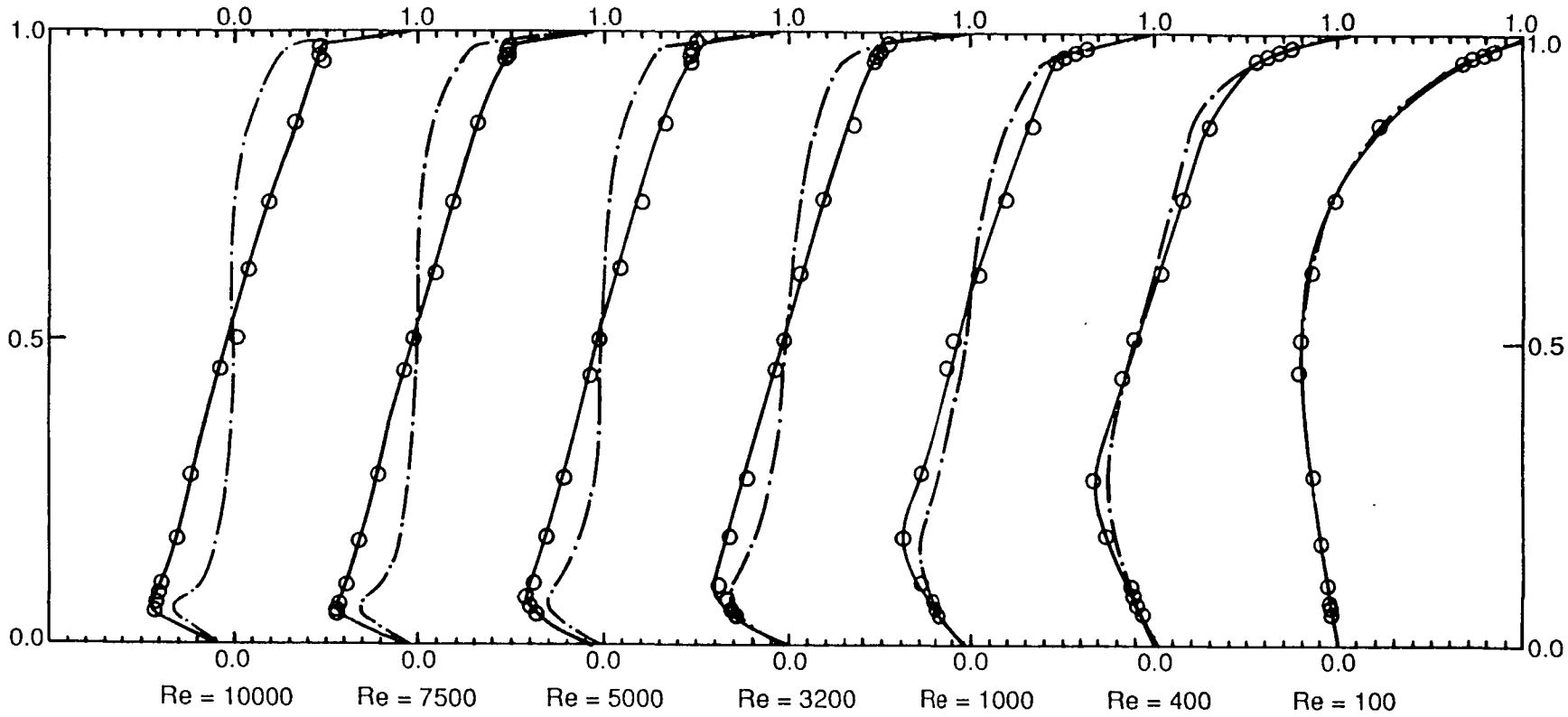

Figure 4. A comparison of u-velocities along a vertical centerline, —: present study without STU, —·—: present study with STU, O: Ghia et al. [18].

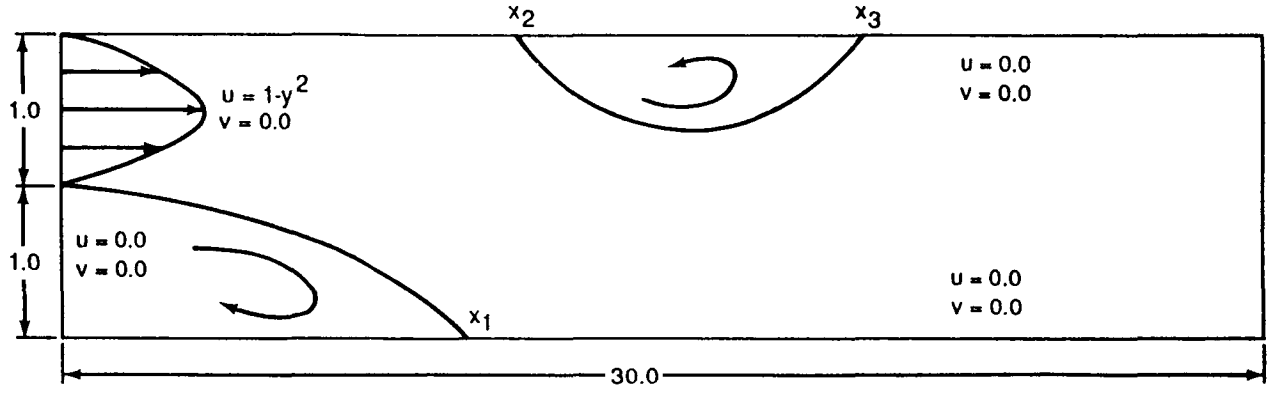

Figure 5. Geometry and boundary conditions of 2-D laminar flow over a backward-facing step.

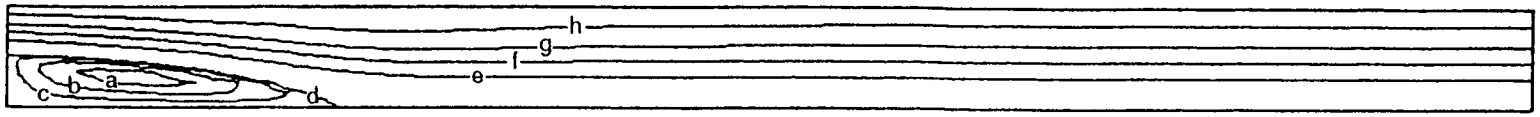

(WITHOUT STU)

(WITH STU)

(a) Re = 300

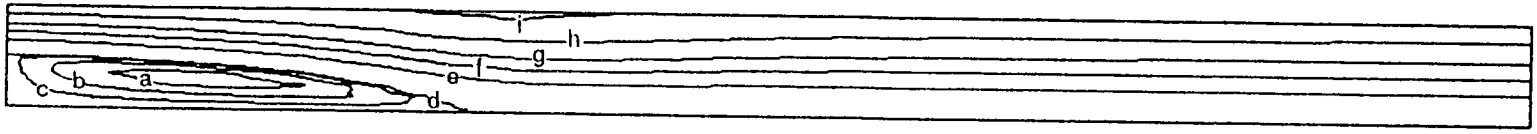

(WITHOUT STU)

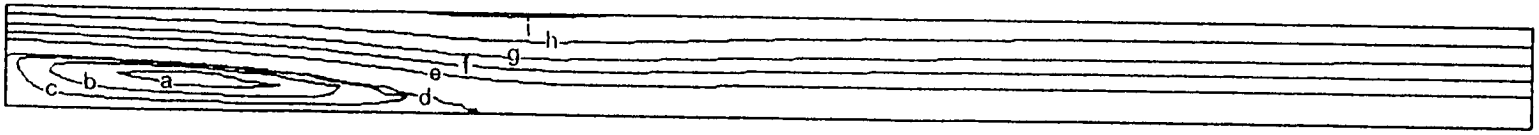

(WITH STU)

(b) Re = 500

Figure 6. Streamline contours of 2-D laminar flow over a backward-facing step.

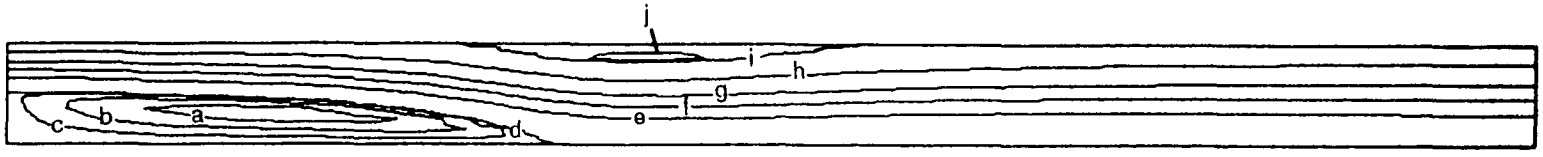

(WITHOUT STU)

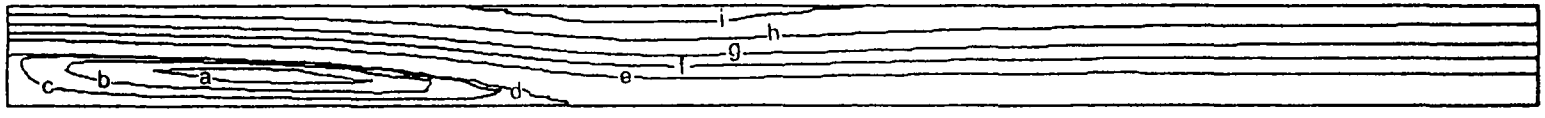

(WITH STU)

(c) Re = 700

Figure 6. (Concluded)

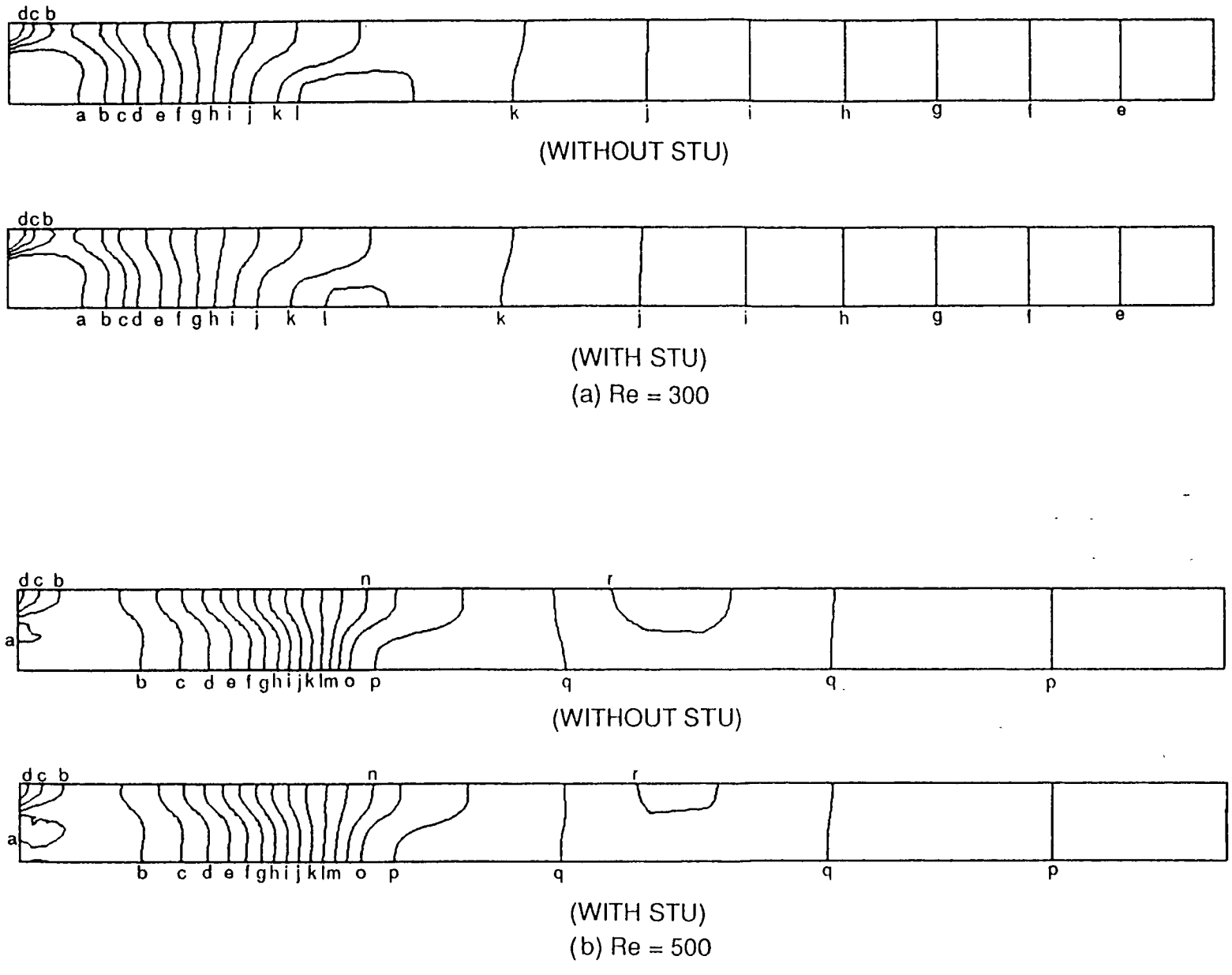

Figure 7. Pressure contours of 2-D laminar flow over a backward-facing step.

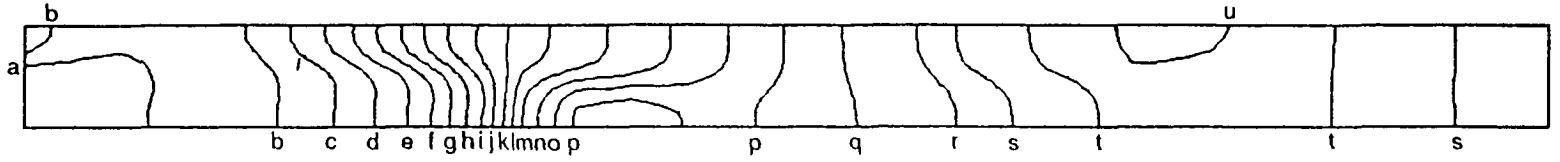

(WITHOUT STU)

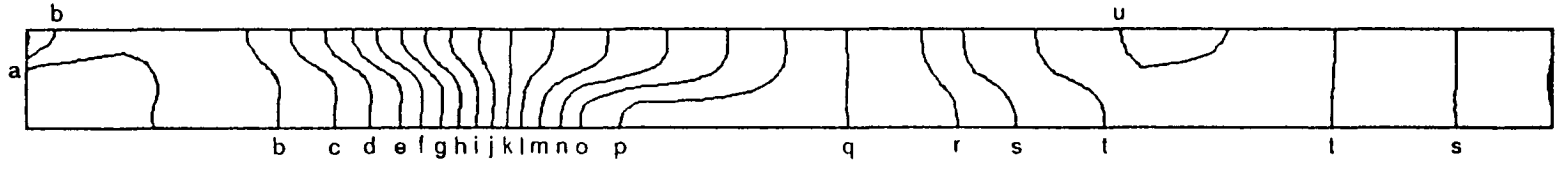

(WITH STU)

(c) Re = 700

Figure 7. (Concluded)

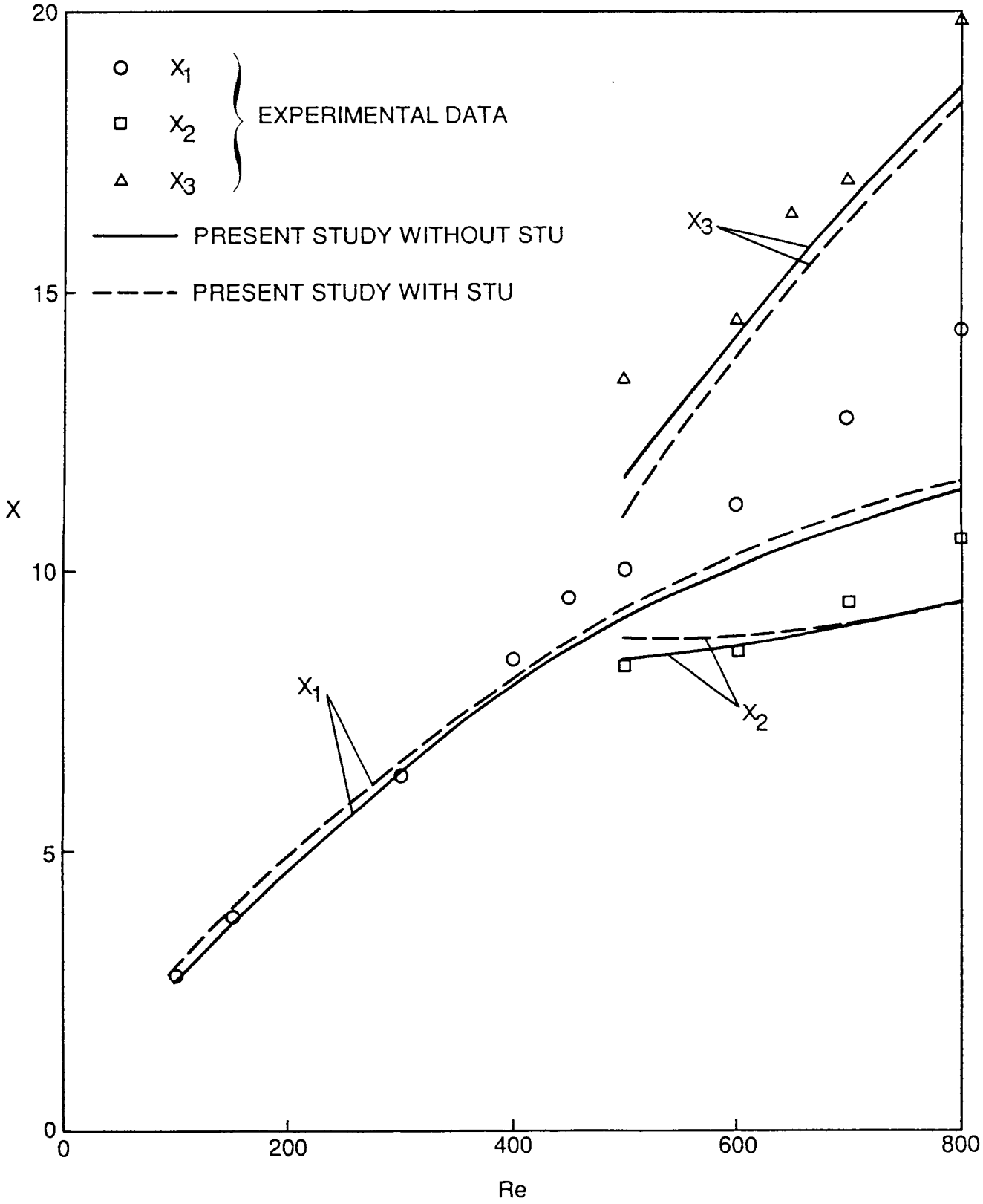

Figure 8. A comparison of reattachment lengths of 2-D laminar flow over a backward-facing step.

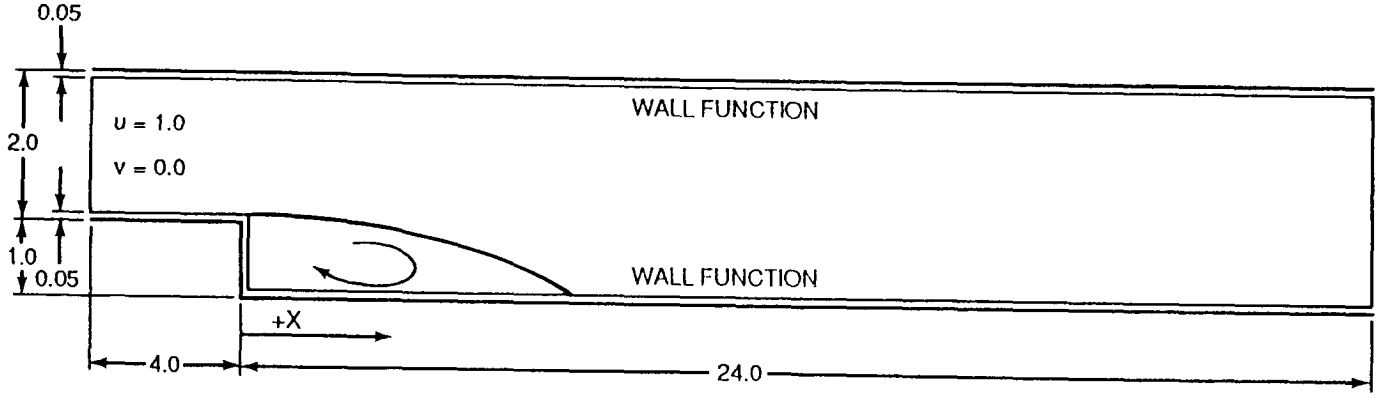

Figure 9. Geometry and boundary conditions of 2-D turbulent flow over a backward-facing step.

Figure 10. Streamline contours of 2-D turbulent flow over a backward-facing step.

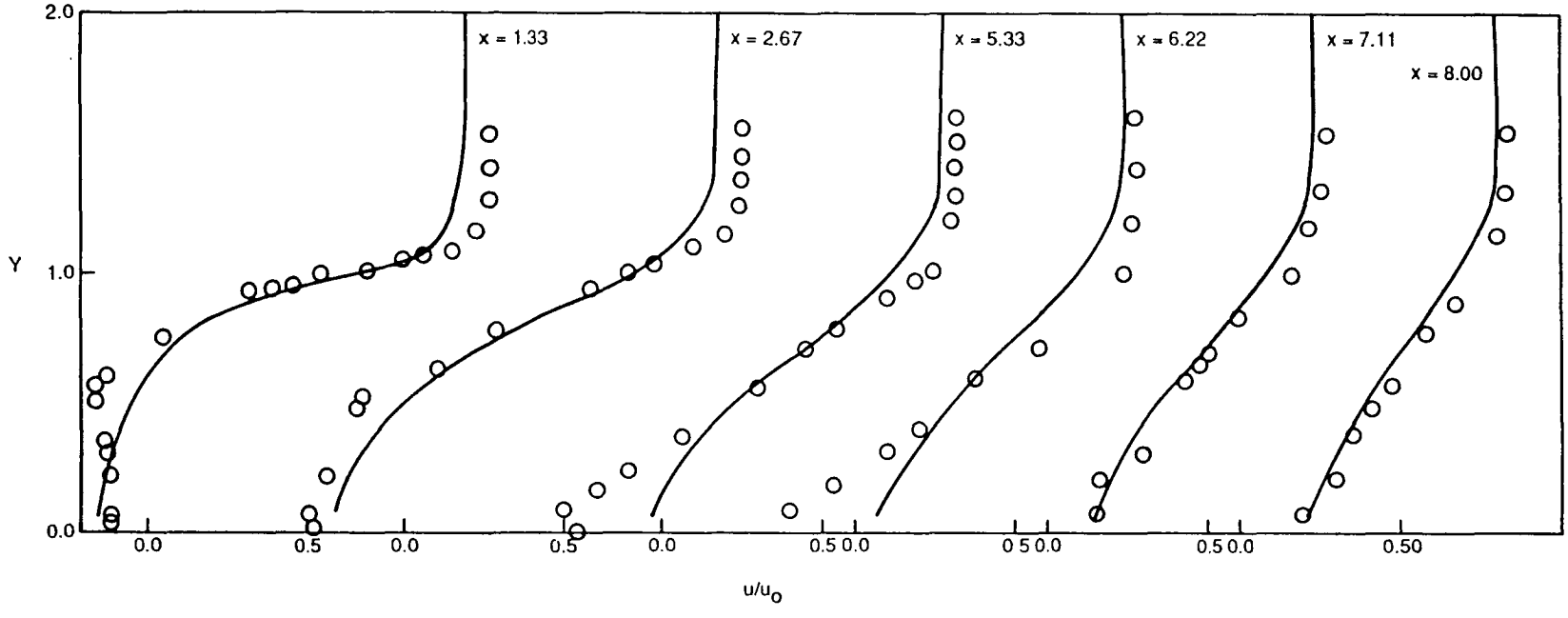

Figure 11. A comparison of predicted and measured velocities for 2-D turbulent flow over a backward-facing step, ——: present study, O: experimental data of Kim et al. [23].

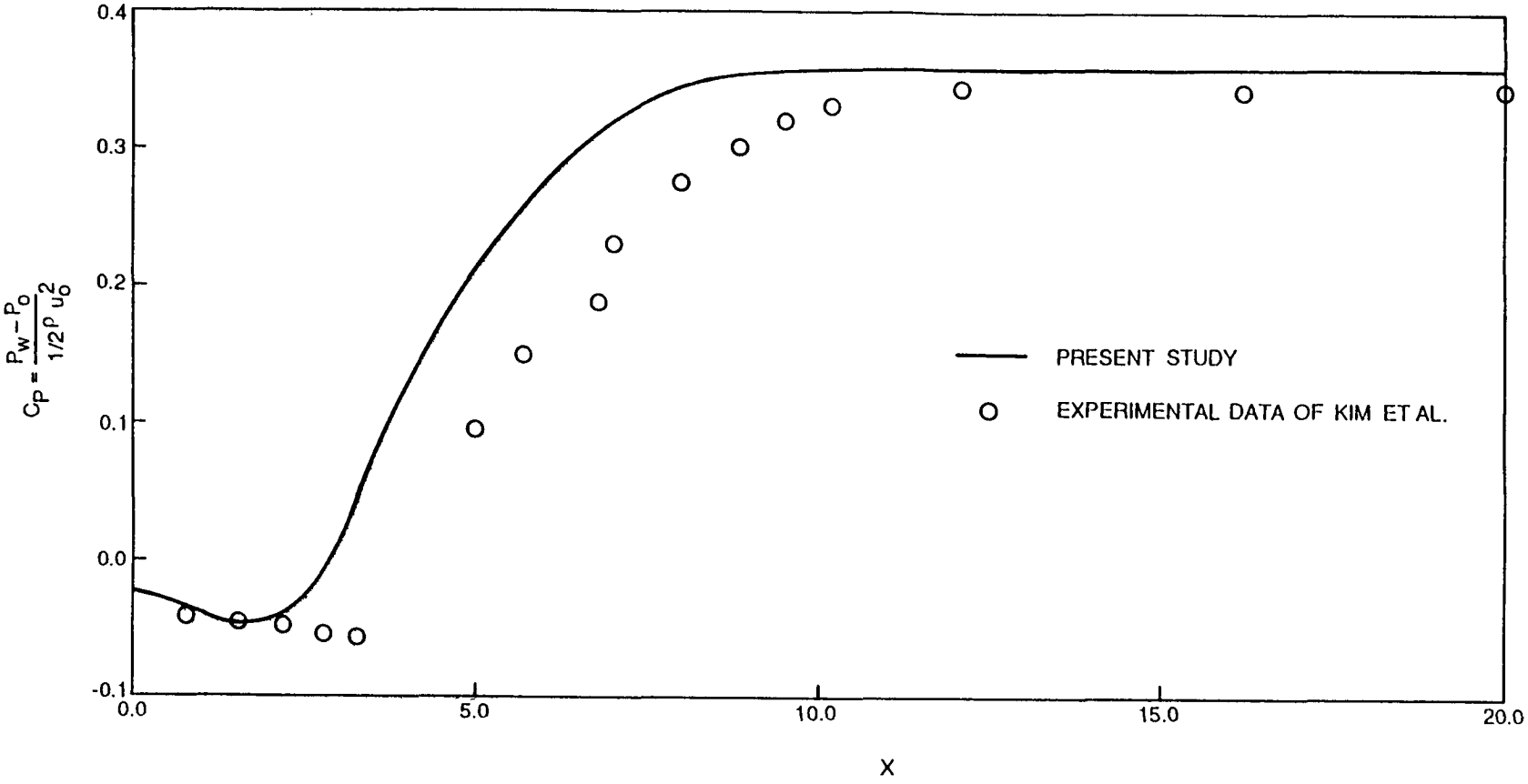

Figure 12. A comparison of predicted and measured pressure coefficient for 2-D turbulent flow over a backward-facing step.

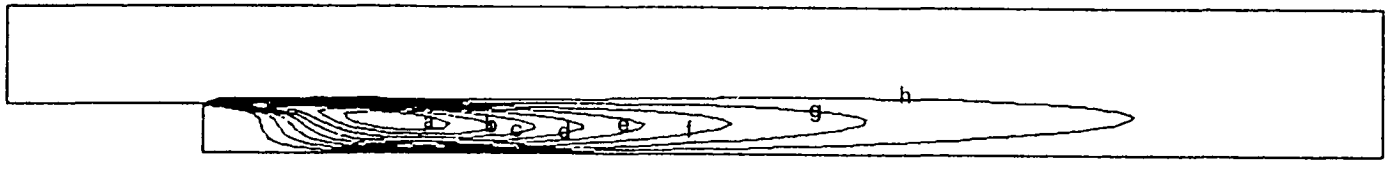

Figure 13. Contours of turbulent kinetic energy of 2-D turbulent flow over a backward-facing step.

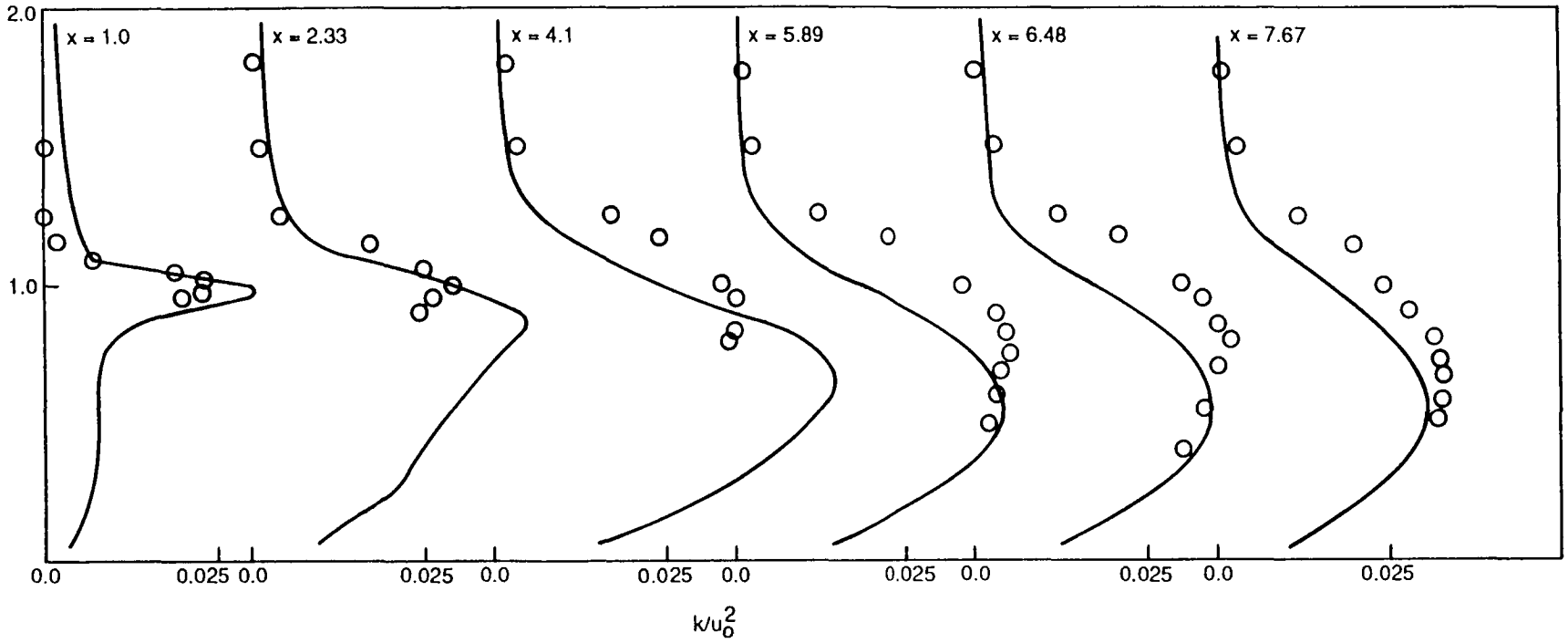

Figure 14. A comparison of predicted and measured turbulent kinetic energy for 2-D turbulent flow over a backward-facing step, ——: present study, O: experimental data of Kim et al. [23].

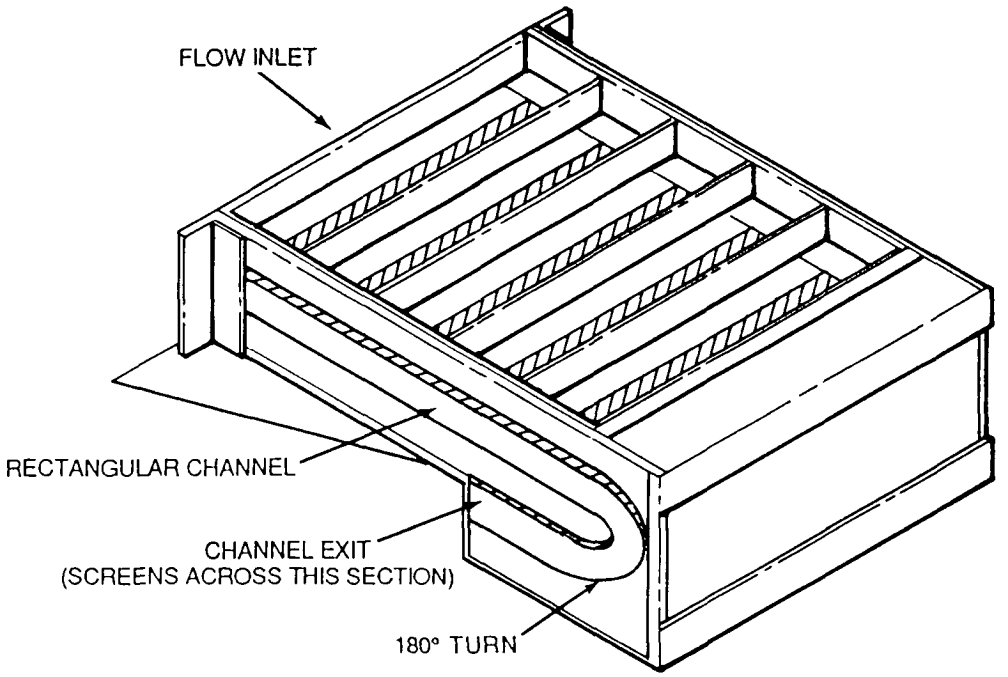

(a) RECTANGULAR TURN-AROUND DUCT

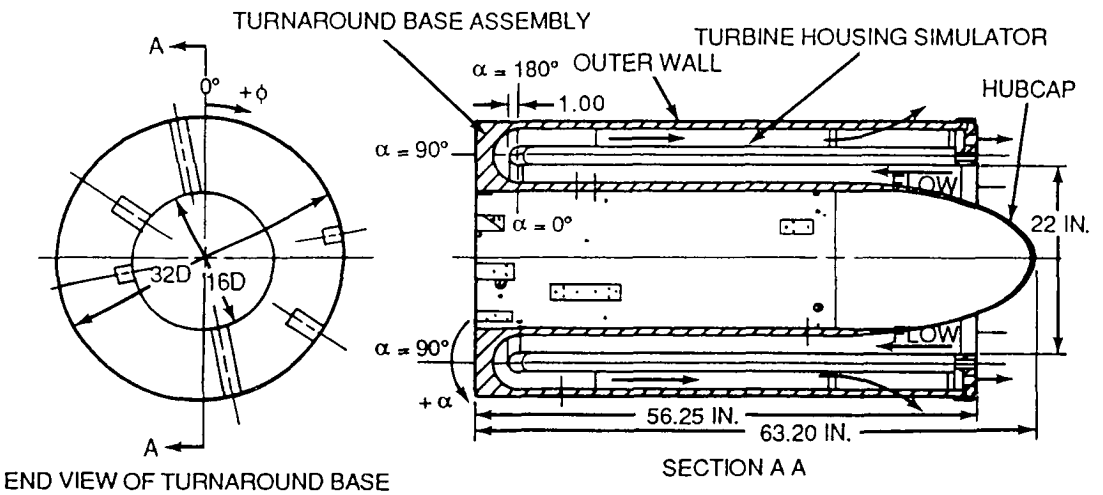

(b) AXI-SYMMETRIC TURN-AROUND DUCT

Figure 15. Experimental apparatus of rectangular and axisymmetric turn-around ducts.

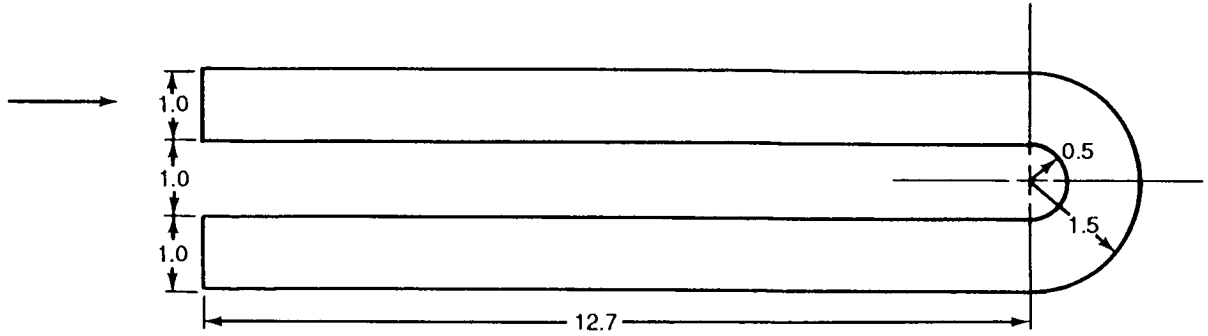

(a) CASE 1

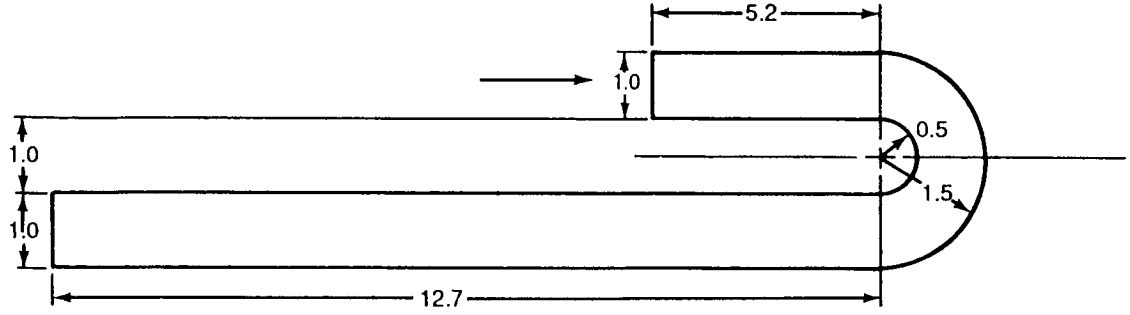

(b) CASE 2

Figure 16. Schematics of the rectangular turn-around duct.

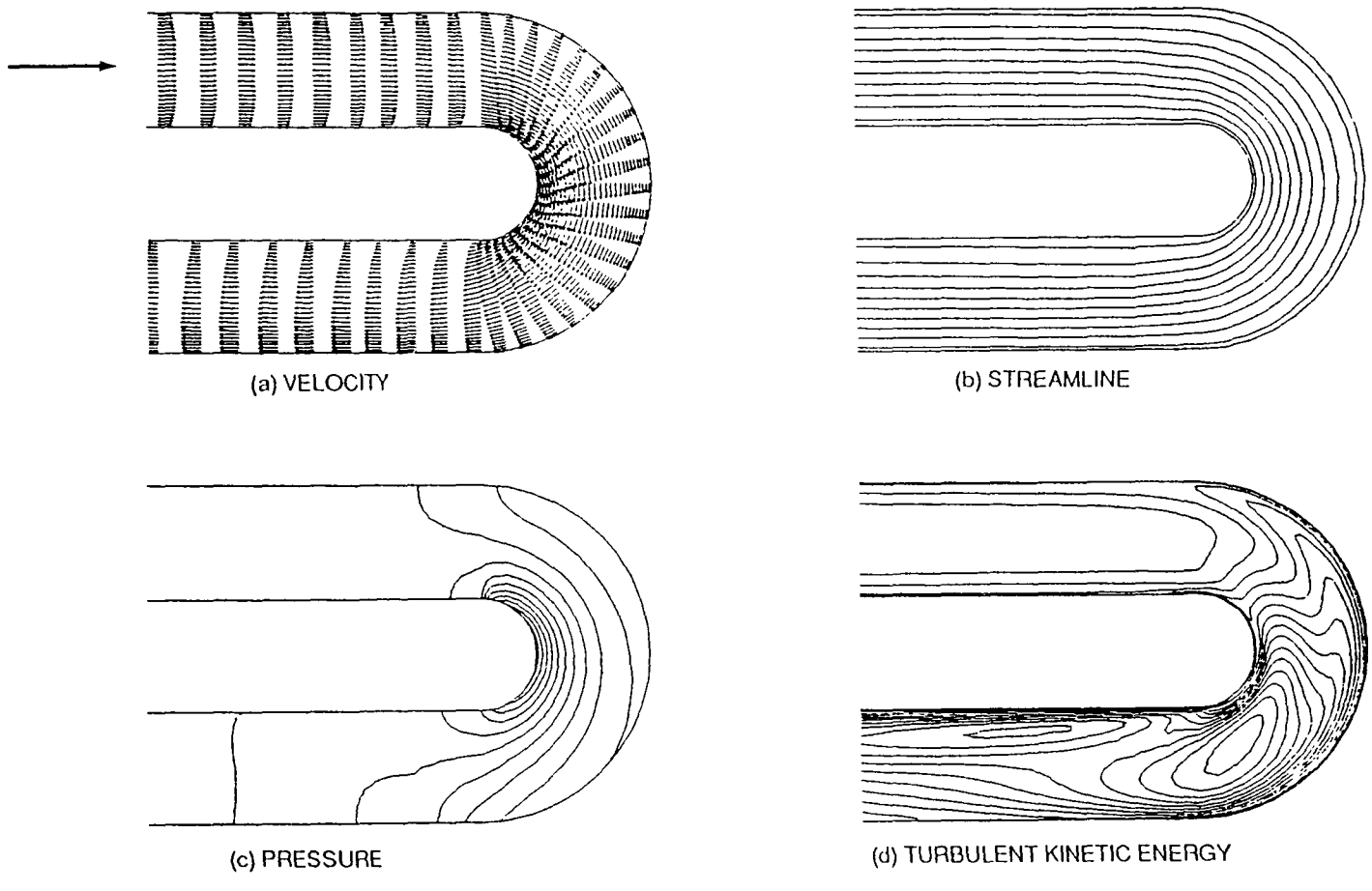

Figure 17. Computational results of 2-D turbulent flow through a rectangular turn-around duct (Case 1).

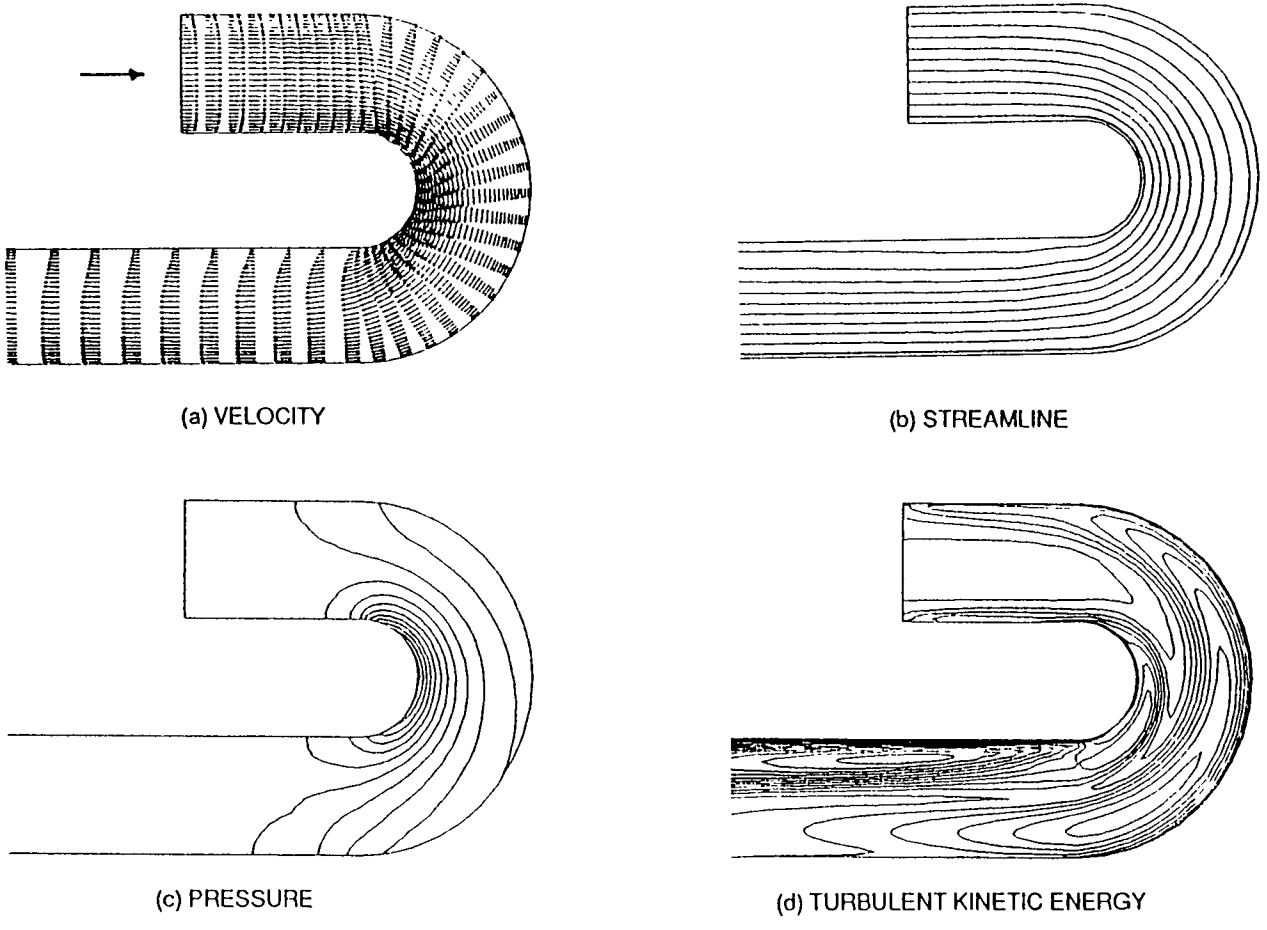

Figure 18. Computational results of 2-D turbulent flow through a rectangular turn-around-duct (Case 2).

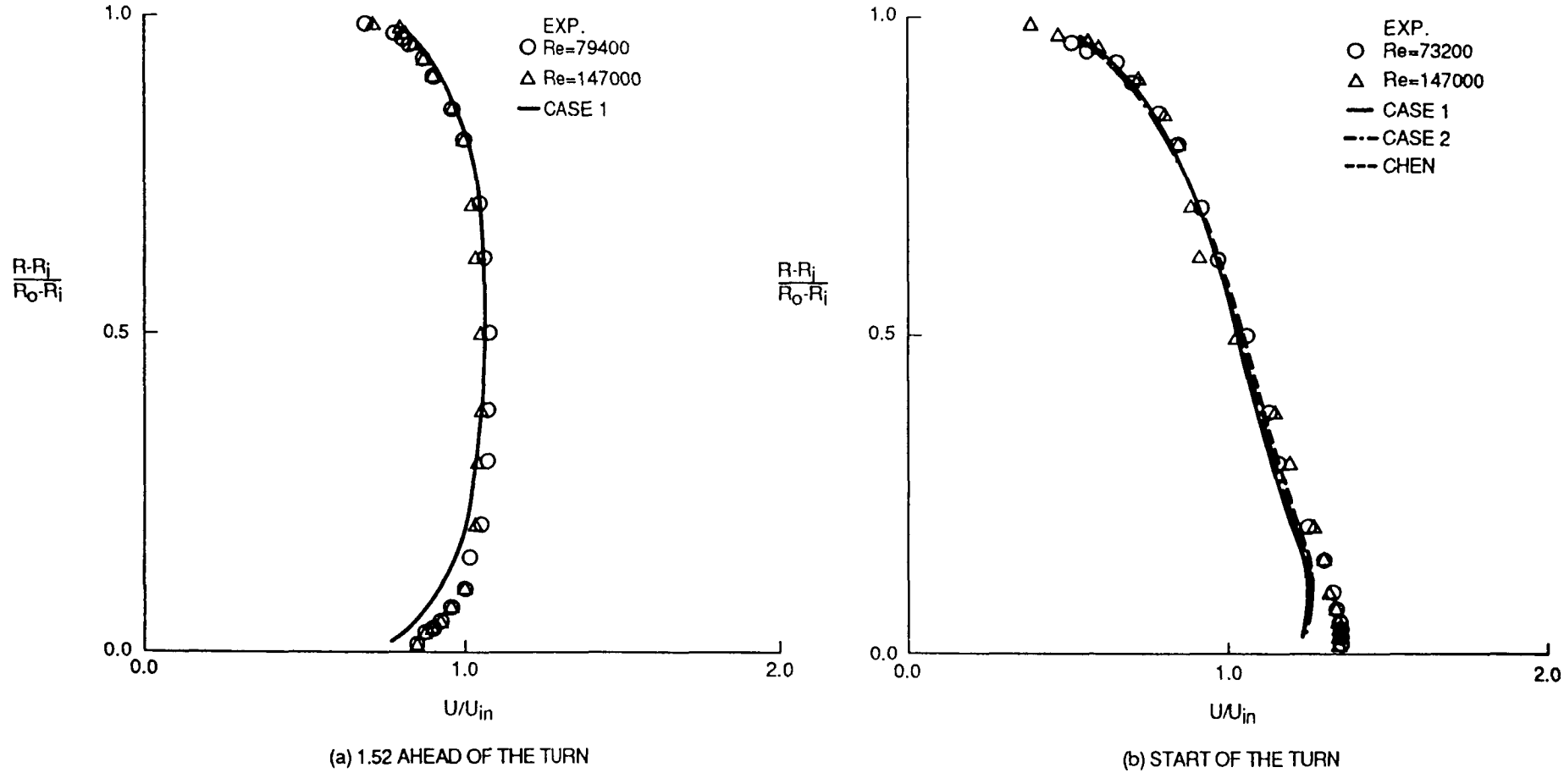

Figure 19. A comparison of predicted and measured mean velocity profiles of 2-D turbulent flow through a rectangular turn-around duct.

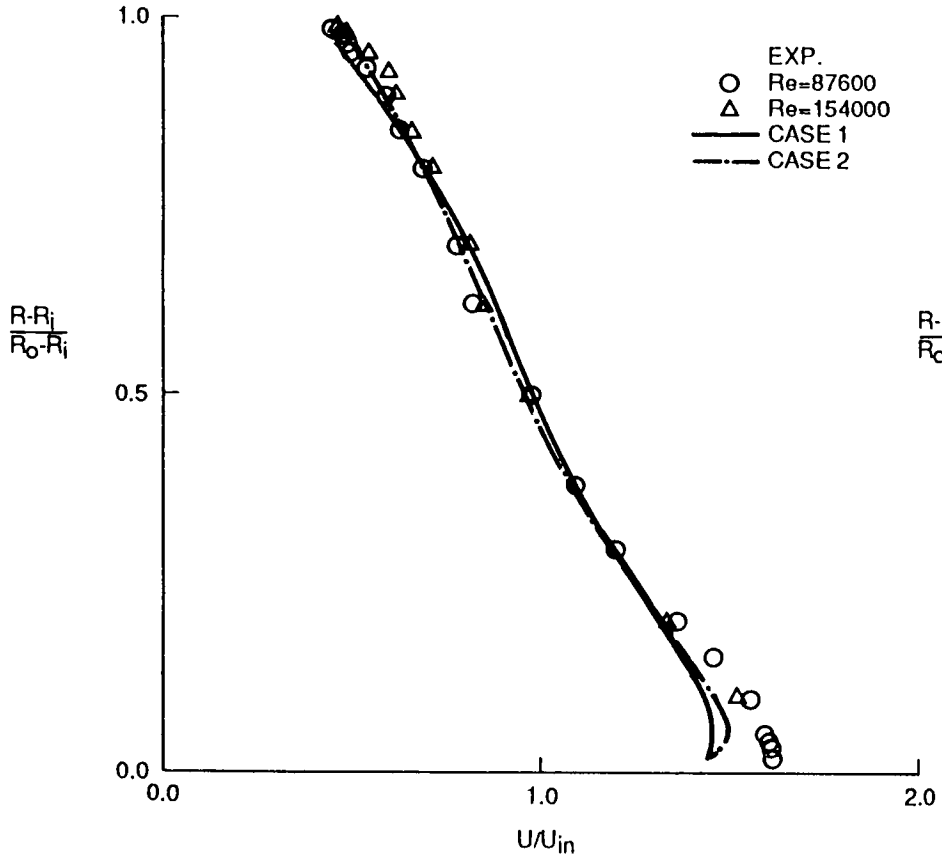

(c) 45° AROUND THE TURN

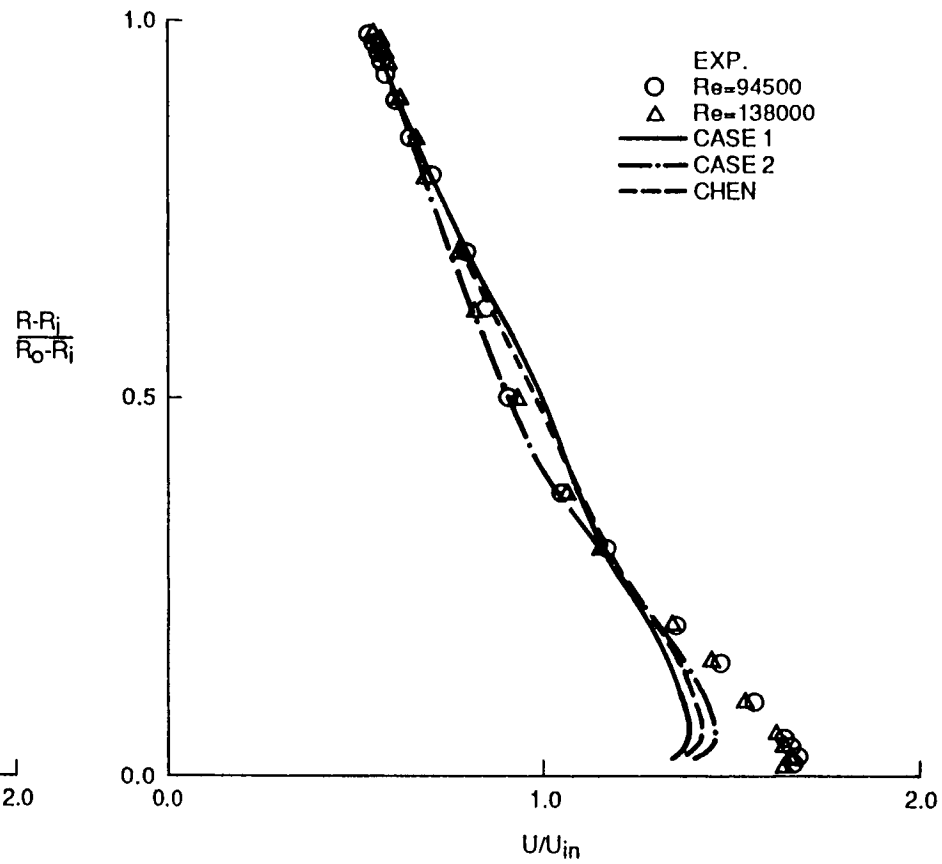

(d) 90° AROUND THE TURN

Figure 19. (Continued)

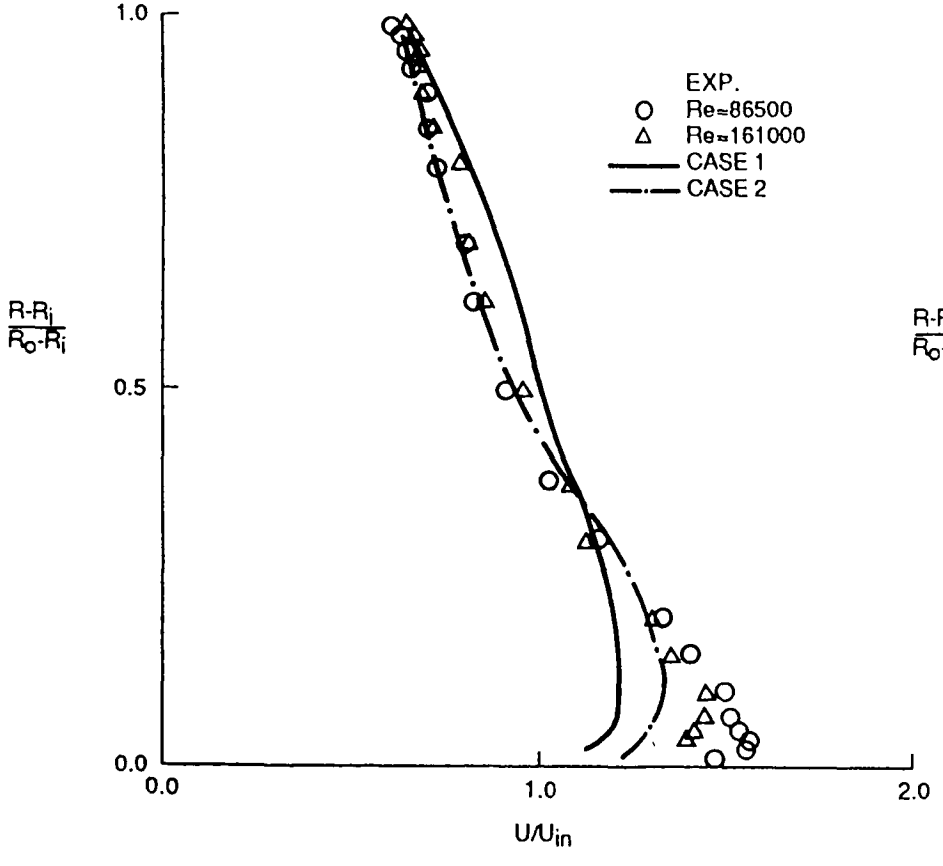

(e) 135° AROUND THE TURN

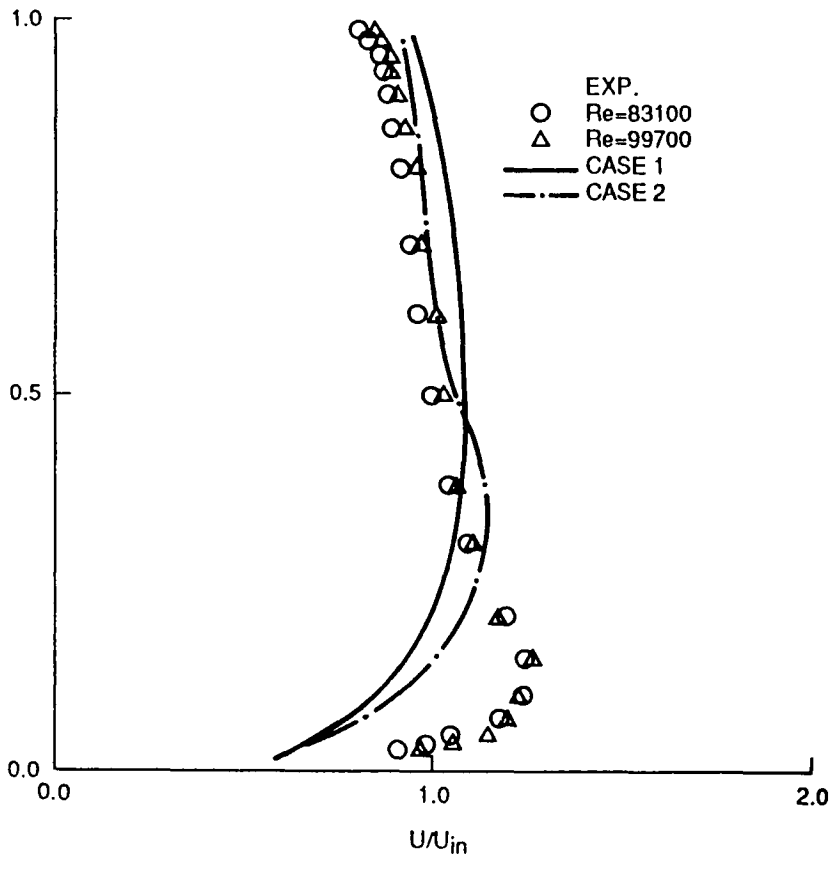

(f) 180° AROUND THE TURN

Figure 19. (Continued)

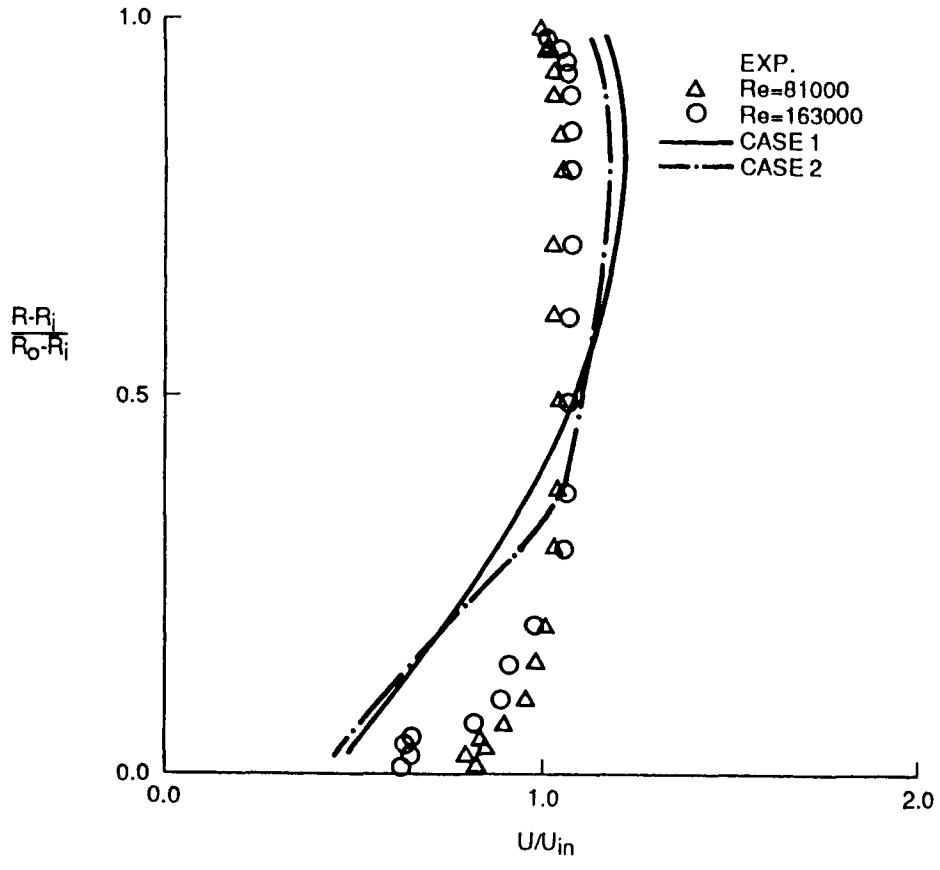

(g) 1.52 DOWNSTREAM OF THE TURN

Figure 19. (Concluded)

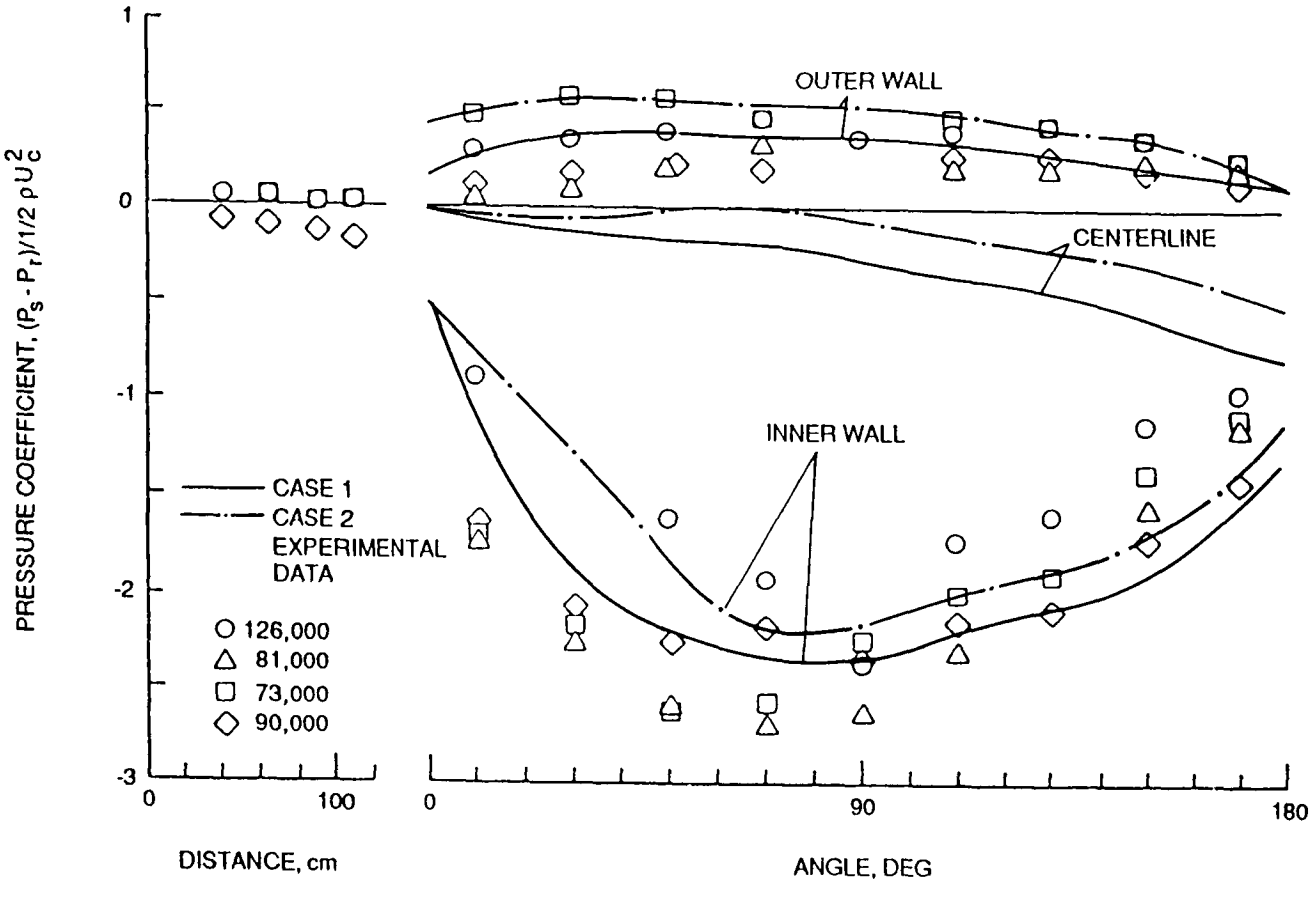

Figure 20. A comparison of predicted and measured pressure coefficients of 2-D turbulent flow through a rectangular turn-around duct.

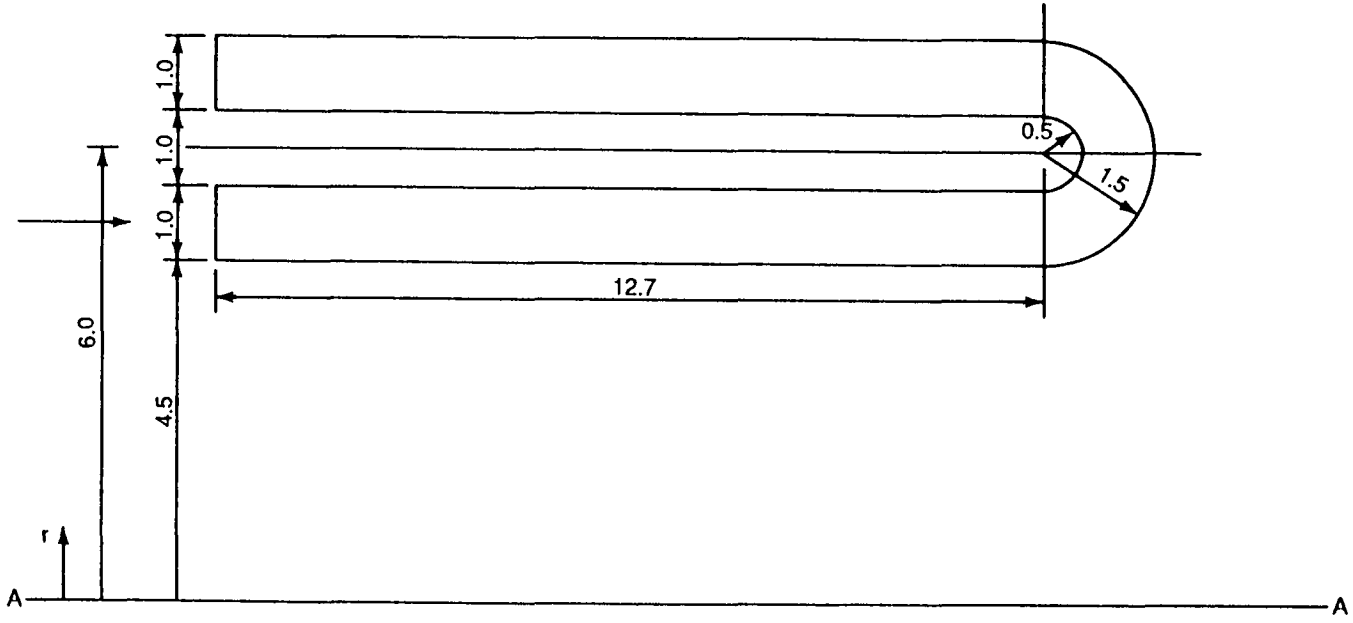

Figure 21. Schematics of the axisymmetric turn-around duct, A-A: centerline of the axisymmetric geometry.

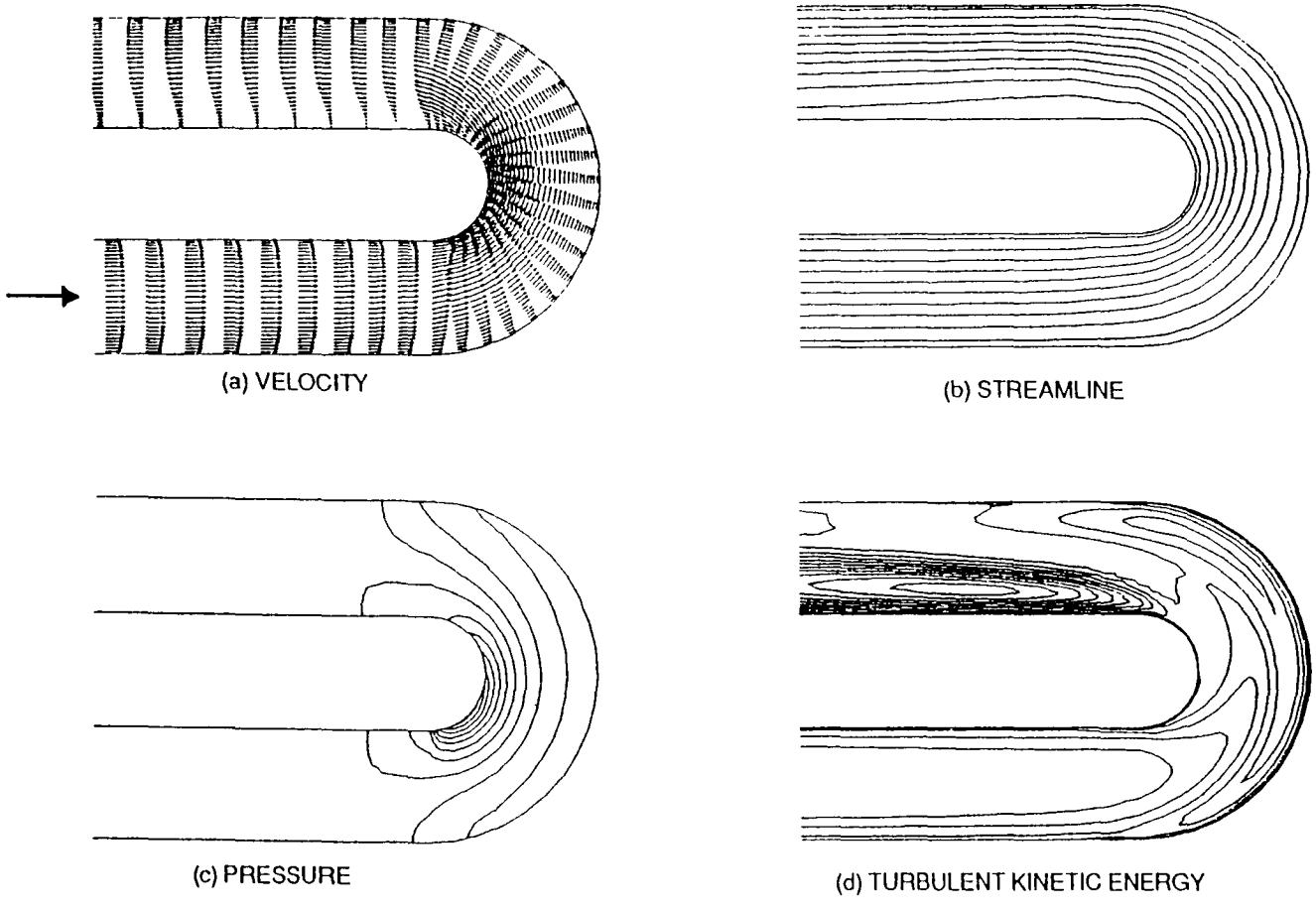

Figure 22. Computational results of 2-D turbulent flow through an axisymmetric turn-around duct.

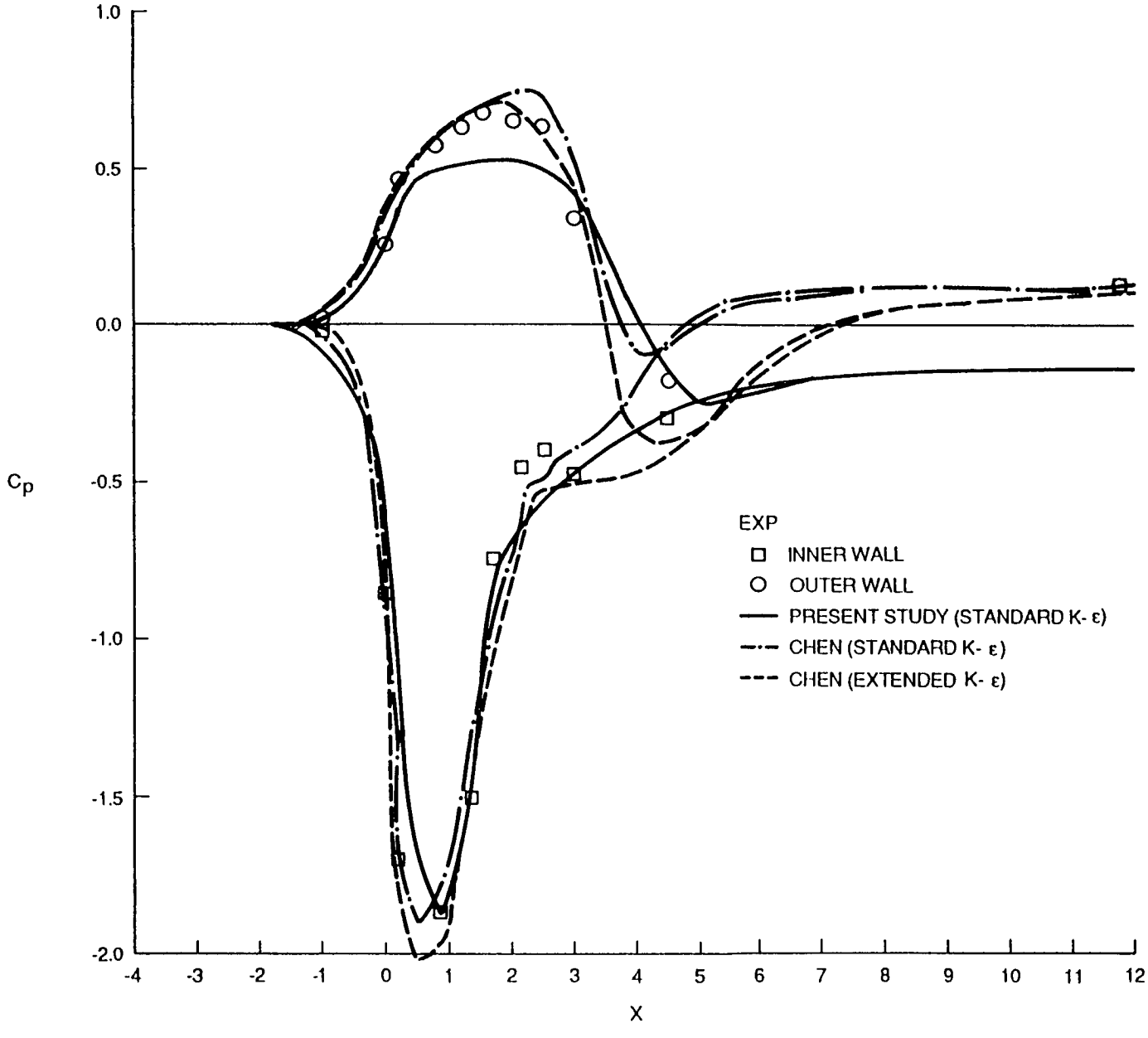

Figure 23. A comparison of predicted and measured pressure coefficients of 2-D turbulent flow through an axisymmetric turn-around duct.

TABLE 1. VALUES OF STREAMLINE AND PRESSURE CONTOURS IN FIGURES 1 AND 3

LABEL	STREAMLINE	PRESSURE
a	-1.0×10^{-10}	-0.1000
b	-1.0×10^{-7}	-0.0900
c	-1.0×10^{-5}	-0.0800
d	-1.0×10^{-4}	-0.0700
e	-0.0100	-0.0600
f	-0.0300	-0.0500
g	-0.0500	-0.0400
h	-0.0700	-0.0300
I	-0.0900	-0.0200
j	-0.1000	-0.0100
k	-0.1100	0.0000
l	-0.1150	0.0100
m	-0.1175	0.0200
n	1.0×10^{-8}	0.0300
o	1.0×10^{-7}	0.0400
p	1.0×10^{-6}	0.0500
q	1.0×10^{-5}	0.0600
r	5.0×10^{-5}	0.0700
s	1.0×10^{-4}	0.0800
t	2.5×10^{-4}	0.0900
u	5.0×10^{-4}	0.1000
v	1.0×10^{-3}	———
w	1.5×10^{-3}	———
x	3.0×10^{-3}	———

TABLE 2. EXTREME VALUES OF STREAM FUNCTIONS AT VARIOUS VORTICES INSIDE A WALL-DRIVEN CAVITY

VORTEX	CASE	REYNOLDS NUMBER						
		100	400	1000	3200	5000	7500	10,000
PR (PRIMARY VORTEX)	PRESENT STUDY WITHOUT STU	-0.102356	-0.111768	-0.115095	-0.115658	-0.114762	-0.113321	-0 112070
	PRESENT STUDY WITH STU	-0.095996	-0 090032	-0.079853	-0.061537	-0.054081	-0.047444	-0 042915
	GHIA ET AL	-0.103423	-0.113909	-0.117929	-0.120377	-0 118966	-0.119976	-0.119731
	GRESHO ET AL			-0.114	-0 118	-0.109	-0.108	-0.101
TL (TOP LEFT)	PRESENT STUDY WITHOUT STU	—	—	—	6.0639×10^{-4}	1.2833×10^{-3}	1.8255×10^{-3}	2.1824×10^{-3}
	PRESENT STUDY WITH STU	—	—	—	$2\,3392\times10^{-5}$	1.9489×10^{-4}	$4\,3026\times10^{-4}$	5.4642×10^{-4}
	GHIA ET AL	—	—	—	7.2768×10^{-4}	1.4564×10^{-3}	2.0462×10^{-3}	2.4210×10^{-3}
	GRESHO ET AL			—	$5\,86\times10^{-4}$	$1\,23\times10^{-3}$	1.84×10^{-3}	2.23×10^{-3}
BL1 (SECOND-ARY BOTTOM LEFT)	PRESENT STUDY WITHOUT STU	1.6913×10^{-6}	1.3244×10^{-5}	2.1730×10^{-4}	1.0447×10^{-3}	1.2533×10^{-3}	1.5534×10^{-3}	1.3732×10^{-3}
	PRESENT STUDY WITH STU	1.5288×10^{-6}	$5\,9496\times10^{-6}$	$9\,4107\times10^{-5}$	$7\,1664\times10^{-4}$	9.4147×10^{-4}	1.0875×10^{-3}	$1\,1390\times10^{-3}$
	GHIA ET AL	1.7488×10^{-6}	1.4195×10^{-5}	2.3113×10^{-4}	$9\,7823\times10^{-4}$	1.3612×10^{-3}	1.4671×10^{-3}	1.5183×10^{-3}
	GRESHO ET AL			2.0×10^{-4}	1.2×10^{-3}	1.49×10^{-3}	1.75×10^{-3}	1.93×10^{-3}
BL2 (TERTIARY BOTTOM LEFT)	PRESENT STUDY WITHOUT STU	—	—	—	$-3\,4498\times10^{-8}$	$-4\,9318\times10^{-8}$	-1.0236×10^{-7}	-4.0672×10^{-7}
	PRESENT STUDY WITH STU	—	—	—	-2.2516×10^{-8}	-3.5332×10^{-8}	$-4\,5713\times10^{-8}$	-9.5564×10^{-8}
	GHIA ET AL	—	-7.6774×10^{-10}	—	$-6\,3300\times10^{-8}$	$-7\,0886\times10^{-8}$	-1.8317×10^{-7}	-7.7565×10^{-7}
	GRESHO ET AL			-1.14×10^{-9}	$-1\,0\times10^{-8}$	-2.85×10^{-8}	-2.74×10^{-7}	-3.08×10^{-8}
BR1 (SECOND-ARY BOTTOM RIGHT)	PRESENT STUDY WITHOUT STU	1.1605×10^{-5}	6.1254×10^{-4}	1.6267×10^{-3}	$2\,6022\times10^{-3}$	2.8014×10^{-3}	2.8585×10^{-3}	$2\,7994\times10^{-3}$
	PRESENT STUDY WITH STU	$9\,3406\times10^{-6}$	$4\,2017\times10^{-4}$	1.1015×10^{-3}	$1\,6599\times10^{-3}$	1.7164×10^{-3}	$1\,6665\times10^{-3}$	1.5897×10^{-3}
	GHIA ET AL	$1\,2537\times10^{-5}$	$6\,4235\times10^{-4}$	$1\,7501\times10^{-3}$	3.1396×10^{-3}	3.0836×10^{-3}	$3\,2848\times10^{-3}$	3.4183×10^{-3}
	GRESHO ET AL			1.76×10^{-3}	3.29×10^{-3}	3.87×10^{-3}	4.86×10^{-3}	5.54×10^{-3}
BR2 (TERTIARY BOTTOM RIGHT)	PRESENT STUDY WITHOUT STU	—	-1.6324×10^{-8}	-4.2032×10^{-8}	$-1\,2434\times10^{-7}$	-7.1179×10^{-7}	-1.4305×10^{-5}	-6.8072×10^{-5}
	PRESENT STUDY WITH STU	—	-1.1556×10^{-8}	$-1\,4968\times10^{-8}$	$-5\,5793\times10^{-8}$	-7.0963×10^{-8}	$-1\,5882\times10^{-7}$	-5.2657×10^{-7}
	GHIA ET AL	—	-1.8659×10^{-8}	$-9\,3193\times10^{-8}$	$-2\,5165\times10^{-7}$	-1.4322×10^{-6}	$-3\,2815\times10^{-5}$	-1.3132×10^{-4}
	GRESHO ET AL			-1.8×10^{-8}	$-2\,05\times10^{-7}$	-5.22×10^{-8}	$-7\,46\times10^{-5}$	$-2\,02\times10^{-4}$

5-299-8-16

TABLE 3. VALUES OF STREAMLINE AND PRESSURE CONTOURS IN FIGURES 6 AND 7

LABEL	STREAMLINE	PRESSURE		
		Re = 300	Re = 500	Re = 700
a	-0.0250	-0.0075	-0.0350	-0.1431
b	-0.0150	-0.0050	-0.0325	-0.0400
c	-0.0050	-0.0025	-0.0300	-0.0375
d	0.0000	-0.0000	-0.0275	-0.0350
e	0.1000	-0.0050	-0.0250	-0.0325
f	0.2000	-0.0100	-0.0225	-0.0300
g	0.3000	-0.0150	-0.0200	-0.0275
h	0.4000	-0.0200	-0.0175	-0.0250
I	0.4391	-0.0250	-0.0150	-0.0225
j	0.4408	-0.0300	-0.0125	-0.0200
k	———	0.0350	0.0100	0.0175
l	———	0.0370	0.0075	0.0150
m	———	———	0.0050	0.0125
n	———	———	0.0025	0.0100
o	———	———	0.0000	0.0075
p	———	———	0.0050	0.0050
q	———	———	0.0100	0.0025
r	———	———	0.0115	0.0000
s	———	———	———	0.0010
t	———	———	———	0.0020
u	———	———	———	0.0025

TABLE 4. VALUES OF STREAMLINE AND TURBULENT KINETIC ENERGY CONTOURS IN FIGURES 10 AND 11

LABEL	STREAMLINE	TURBULENT KINETIC ENERGY
a	-0.0600	0.0450
b	-0.0400	0.0400
c	-0.0200	0.0350
d	0.0000	0.0300
e	0.2000	0.0250
f	0.4000	0.0200
g	0.6000	0.0150
h	0.8000	0.0100
i	1.0000	———
j	1.2000	———
k	1.4000	———
l	1.6000	———
m	1.8000	———

☆U.S. GOVERNMENT PRINTING OFFICE: 1988 - 530-050/80109

TECHNICAL REPORT STANDARD TITLE PAGE

1. REPORT NO.	2. GOVERNMENT ACCESSION NO.	3. RECIPIENT'S CATALOG NO.
NASA CR-179390		

4. TITLE AND SUBTITLE	5. REPORT DATE
Numerical Analysis of Laminar and Turbulent Incompressible Flows Using the Finite Element "Fluid Dynamics Analysis Package (FIDAP)"	August 1988
	6. PERFORMING ORGANIZATION CODE
7. AUTHOR(S)	8. PERFORMING ORGANIZATION REPORT #
Jeong L. Sohn	
9. PERFORMING ORGANIZATION NAME AND ADDRESS	10. WORK UNIT NO.
Universities Space Research Association 4950 Corporate Dr., Suite 100 Huntsville, Alabama 35806	11. CONTRACT OR GRANT NO. NAS8-35918
12. SPONSORING AGENCY NAME AND ADDRESS	13. TYPE OF REPORT & PERIOD COVERED
National Aeronautics and Space Administration Washington, D.C. 20546	Final Contractor Report
	14. SPONSORING AGENCY CODE

15. SUPPLEMENTARY NOTES

Prepared by Fluid Dynamics Branch (ED42), Earth Science and Application Division, Structures and Dynamics Laboratory, Science and Engineering Directorate.

16. ABSTRACT

The purpose of the present study si the evaluation of the numerical accuracy of FIDAP. Accordingly, four test problems in laminar and turbulent incompressible flows are selected and the computational results of these problems are compared with other numerical solutions and/or experimental data. These problems include: (1) 2-D laminar flow inside a wall-driven cavity, (2) 2-D laminar flow over a backward-facing step, (3) 2-D turbulent flow over a backward-facing step, and (4) 2-D turbulent flow through a turn-around-duct.

17. KEY WORDS	18. DISTRIBUTION STATEMENT
Laminar, Turbulent, Incompressible Finite Element Method	Unclassified/Unlimited

19. SECURITY CLASSIF. (of this report)	20. SECURITY CLASSIF. (of this page)	21. NO. OF PAGES	22. PRICE
Unclassified	Unclassified	59	NTIS